REVERSIBILITY AND KINETIC PRECIPITATION OF ASPHALTENES

by

Wattana Chaisoontornyotin

A dissertation submitted to the faculty of
The University of Utah
in partial fulfillment of the requirements for the degree of

Doctor of Philosophy

Department of Chemical Engineering

The University of Utah

December 2017

The University of Utah Graduate School

STATEMENT OF DISSERTATION APPROVAL

The dissertation of **Wattana Chaisoontornyotin**

has been approved by the following supervisory committee members:

Michael P. Hoepfner	, Chair	**07/20/2017** Date Approved
Milind Deo	, Member	**07/20/2017** Date Approved
Mikhail Skliar	, Member	**07/20/2017** Date Approved
John David Mclennan	, Member	**07/20/2017** Date Approved
Keunhan Park	, Member	**07/20/2017** Date Approved

and by **Milind Deo** , Chair/Dean of

the Department/College/School of **Chemical Engineering**

and by David B. Kieda, Dean of The Graduate School.

ABSTRACT

Asphaltenes are one of the component fractions in crude oil and can destabilize due to a change of pressure, temperature, or composition. Destabilized asphaltenes can precipitate and deposit, causing numerous problems and challenges during oil production and processing such as plugging, fouling, and emulsion stability. Thermodynamic models were previously developed to investigate and predict the phase behavior of asphaltenes using experimental data that assumed the destabilized asphaltenes reach their equilibrium state immediately after changing system conditions. However, asphaltene precipitation has previously been shown to be a slow aggregation process suggesting that the previous thermodynamic models might be inaccurate and misrepresent the behavior of asphaltenes.

Reversibility is a requirement for the application of equilibrium thermodynamics to predict the phase behavior of mixtures. In this work, asphaltene precipitation was found to be a reversible process, and the cause of the partial reversibility conclusion in previous work was discovered to be a neglected slow aggregation process. This finding reinforces the importance of a slow aggregation process as it shows that considering the kinetics can significantly alter the conclusions.

The aggregation rates of asphaltenes have also previously been investigated and found that the aggregation rates of asphaltenes depend on thermodynamic driving forces. This study shows that asphaltene aggregation and deposition highly correlate with thermodynamic driving forces, but the deposit growth was governed by diffusion limitations. This investigation reveals that thermodynamic properties can directly

investigate the asphaltene behavior, and the diffusion limitation finding can lead to developing a new and more accurate deposition model.

In addition, for the first time, the presence of inorganic solids was observed to increase the rate of asphaltene precipitation. A model was developed to quantify the rate of asphaltene precipitation under different process conditions. This investigation leads to a clearer understanding of the complex asphaltene aggregation process that occurs in real and heterogeneous systems. The usages of inorganic solids as nucleation sites to remove unstable asphaltenes and decrease the asphaltene problems during the production are potentially possible.

The findings from this dissertation emphasize the essentials of precipitation kinetics and provide ideas to decreases the asphaltene problems and understanding the behavior of asphaltenes using the thermodynamic properties.

To my loving and supportive parents, Somchai and Narumon Chaisoontornyotin.

TABLE OF CONTENTS

LIST OF FIGURES

Figures

LIST OF TABLES

Tables

ACKNOWLEDGEMENTS

This work would not have been possible without many individual contributors who encouraged and supported me along this challenging and enjoyable journey. I have gained many valuable experiences and knowledge in both professional and life skills. I have been fortunate to come across many wonderful people who have contributed to my success in different ways.

I would first like to express my gratitude to my advisor Professor Michael P. Hoepfner, who is a great advisor and fabulous mentor. He has assisted me in my research and helped me develop myself as an independent researcher. I was the very first person who joined his research group, and I am really thankful for all of the opportunities that I have been offered. He always motivates the students and supports innovative and creative ideas. Undoubtedly, I have been very fortunate to be in his group.

I am grateful and thankful for my committee members: Professors Milind Deo, Mikhail Skliar, John David Mclennan, and Keunhan Park, who have provided valuable insights and input to improve and increase the quality of my research. In addition, I would like to thank Professors Milind Deo and John David Mclennan for the numerous suggestions and assistance with applying for job positions. I would also like to thank Syncrude Canada Limited for their financial support in my project. I also would like to acknowledge my appreciation to the Department of Chemical Engineering staff who have assisted me in general: Ribana Milas, Cynthia Ruiz, and Christina Bushman.

I would like to thank all my colleagues in the research group for creating a friendly

and helpful environment: Yuan Yang, Siddharth Agrawal, Weiyi Kong, Austin W. Bingham, Jingzhou Zhang, and Amanda Chew. I would like to especially thank Yuan Yang who joined the same research group one semester later than me. I am grateful for our research and life discussions. Austin W. Bingham and Jingzhou Zhang have been a great help on research, and I am really happy to work with them. Moreover, I have also been extremely lucky to meet HyeYoung Cho, Luanjing Guo, and many people here in Salt Lake City. My study life would be different without them.

I would like to express my deepest gratitude for my parents, Somchai and Narumon Chaisoontornyotin for their love, support, encouragement, and trust throughout my life. I would not be here and be who I am today without them. I would also like to thank my brother, Naruchit Chaisoontornyotin, for his support. Lastly, I would like to thank Jiye Lee for her caring and support, and I have been very fortunate to meet and spend time with her.

CHAPTER 1

INTRODUCTION

1.1 Asphaltenes

The global liquid fuels consumption was approximated at 90 million barrels per day (b/d) in 2012 and has since been increasing.[1] The consumption is predicted to be 100 and 121 million b/d in 2020 and 2040, respectively.[1] Crude oil and condensate production were 80% of all-liquids fuels,[2] and the current global oil value is estimated at $90 trillion in the ground.[3] Crude oil is a complex mixture of hydrocarbons and consist of saturates, aromatics, resins, and asphaltenes called SARA fractions.[4–8] Asphaltenes are defined as the heaviest oil fraction, and they are soluble in aromatics solvent (e.g., toluene) and insoluble in n-alkanes (e.g., n-heptane).[5,7,9–21] A change of pressure, temperature, or composition during operation of wells can destabilize asphaltenes.[4,22–24] Destabilized asphaltenes can precipitate and deposit in processing and refining equipment leading to decreases in oil productivity, production downtime, and downstream issues such as fouling in heat exchangers.[4,7,13,17,25] The removal cost of deposited asphaltenes in the near well bore for a deepwater well can be around $3 million plus $1.2 million US dollars of the production lost per day.[26]

Various techniques have been utilized to measure the molecular weight of asphaltenes such as mass spectrometry and molecular diffusion.[27,28] The mass spectrometry methods such as two-step laser mass spectrometry[29] and laser desorption ionization

(LDI)[30,31] measures the charge-to-mass ratio by inducing a charge on the molecule. The molecular diffusion techniques such as time-resolved fluorescence depolarization (TRFD)[31,32] and fluorescence correlation spectroscopy (FCS)[31,33] measure a diffusion constant and relate to molecular mass by comparison with model compounds. Both mass spectrometry and molecular diffusion techniques have provided similar results that the average molecular weight of asphaltenes can range from 300 to 1,400 g/mol. The two most accepted structure models of asphaltenes are the continental or island model and the archipelago model.[34–37] The island model is composed of a condensed polycyclic aromatic hydrocarbon core with a shell of alkyl side chains as shown in Figure 1.1a.[34,35,37] For the island model, the interaction between the polyaromatics core generates an attraction force for aggregation that is limited by the steric repulsions between the aliphatic chains surrounding the aromatic core.[34,38] Figure 1.1b demonstrates the archipelago model, which consists of several aromatic cores that are connected by alkyl chains[34–37], and asphaltene aggregation occurs by bridging and hydrogen bonding.[34] However, rather than investigate the fundamental structure and behavior of asphaltenes in the micro scale, which is in nanometer length, asphaltene precipitation in the macro scale was focused on this study.

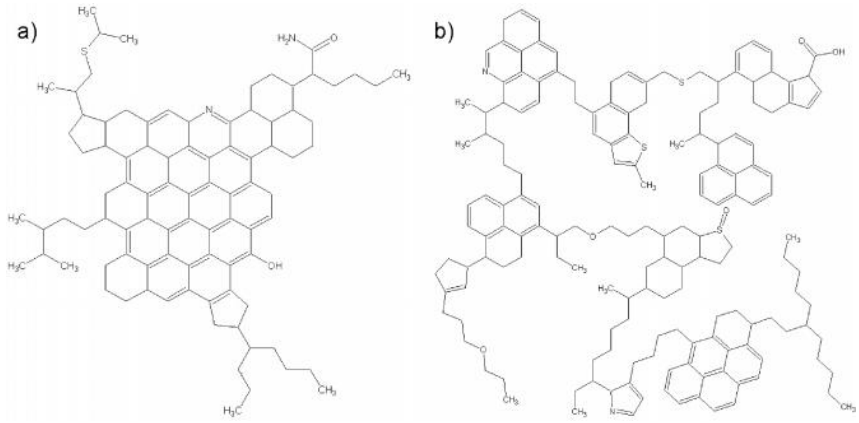

Figure 1.1 Structure models of asphaltenes: island model (a) and archipelago model (b).[34]

1.2 Asphaltenes Precipitation

Asphaltene precipitation is extensively investigated. A common technique to study asphaltene destabilization is to add a diluent/precipitant (e.g., naphtha or n-alkanes) to a crude oil/bitumen to induce precipitation in the laboratory.[21,39,40] Normally, n-pentane or n-heptane is added to crude oil at a volume ratio of 40:1, which is the ASTM D2007 standard, to measure the asphaltene content in the solution. The destabilized asphaltenes at the 40:1 ratio are named after the precipitant used, such as pentane-asphaltenes and heptane-asphaltenes. Using the lower carbon number of n-alkanes as precipitants increases the amount of precipitated asphaltenes.[41] However, lower carbon number precipitants have a higher propensity to evaporate, which adds experimental difficulty. In order to perform experiments accurately and conveniently, n-heptane is usually used as an asphaltene precipitant for laboratory studies.

Different techniques such as optical microscopy,[7,40,42] ultraviolet-visible (UV-vis) spectroscopy,[43] and refractive index measurements[42,44] have been used to detect the instability of asphaltenes. Previous work[7,40,45] used n-alkanes as a precipitant to destabilize asphaltenes, and the quantity of asphaltenes precipitating as a function of time was monitored. Asphaltene precipitation was found to take weeks or months to be detected at sufficiently low precipitant concentrations indicating a slow kinetic aggregation process.[7,21,42,46] A larger size and higher mass of precipitated asphaltenes were observed as time passed using an optical microscopy and a centrifugation-based separation technique as shown in Figure 1.2. At higher heptane concentrations, asphaltene destabilization may be detected over shorter experimental durations but an accurate measurement of the asphaltene solubility may require additional time.[7,40] This finding has revealed that asphaltene precipitation does not only depend on precipitant and precipitant concentration,

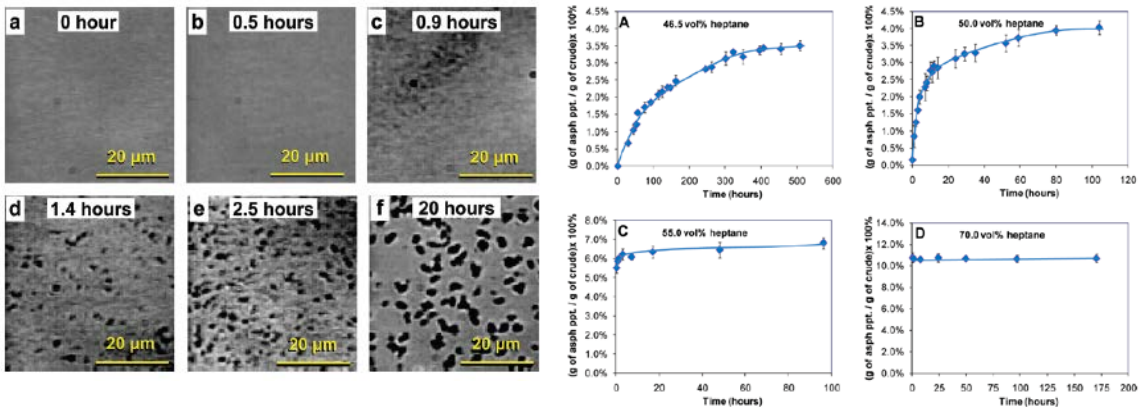

Figure 1.2 Results demonstrate the kinetic precipitation of asphaltenes.[40] Left: Precipitated asphaltenes images in 50 vol % heptane in K-1 oil as a function of time using an optical microscope.[40] Right: Mass percentage of asphaltenes precipitated for K-1 oil as a function of time for different heptane concentrations using a centrifugation-based separation technique.[40]

but there are also kinetic delays to the results playing an important role.

Experiment conditions used to investigate asphaltene precipitation are normally limited due to the limitation of techniques. Thermodynamic models have been developed to investigate and predict the phase behavior of asphaltenes at the full range of conditions. The assumption that solution instantly reached the equilibrium state after adding a precipitant was normally applied, and the experimental data were used to develop the thermodynamic models.[44,47] However, as discussed that asphaltene precipitation is a slow aggregation process, the results and conclusions of previous work might not be reliable and should be questioned due to neglecting the slow kinetic precipitation. Neglecting the kinetic effects can result in inaccurate measurement of the asphaltene stability region and solubility, which is the essential data for developing the model, resulting in misleading thermodynamic models and conceptual understanding of asphaltene behavior.

Another misleading conclusion is that thermodynamic models that have been used to investigate asphaltene phase behavior have been developed by assuming that asphaltene precipitation is a reversible process. Reversibility is a requirement for the application of

equilibrium thermodynamics to predict the phase behavior of mixtures.[48,49] However, previous work has demonstrated that using pressure and composition-induced aggregation, asphaltene precipitation is a reversible process, but only partially reversible using temperature changes.[4,11,12,47,50–58] Therefore, in order to be able to develop the thermodynamic model, asphaltene reversibility should be reinvestigated, and the experimental data needs to take into account the slow aggregation process of asphaltenes. The finding of reversibility can suggest whether the thermodynamic models are appropriate to investigate the phase behavior of asphaltenes. If the asphaltene precipitation is not a reversible process, the colloidal models, which assume an irreversible process of asphaltene precipitation, might be more suitable.

1.3 Asphaltene Precipitation With Surfaces

Previous work[45,46,59] has demonstrated that the aggregation rates of asphaltenes from the slow aggregation process depend on thermodynamic driving forces tested with various crude oils, model oils, and n-alkanes. The thermodynamic driving force was found to be able to estimate and predict the aggregation rates of asphaltenes. Asphaltene deposition such as asphaltenes deposited inside a pipeline also normally occurs during oil production, but asphaltene deposition has not been investigated whether such relationship is also present. The results from previous work[45,46,59] suggest that the relationships between kinetic aggregation, deposition, and thermodynamic driving forces might also exist, but it is still not clear. The finding of the relationship can result in a better understanding of the properties that govern asphaltene aggregation, deposition, and growth processes, which can better help develop the model to predict the asphaltene behavior.

Asphaltenes cannot only deposit inside the pipeline but also deposit on inorganic solids, which are generally present in the bitumen extraction process.[25,37,60,61] The difference between bitumen and crude oil can be indicated by the density.[8] The density of bitumen and crude oil are >1,000 and 815-855 kg/m^3, respectively.[8] The bitumen can be extracted from oil sand, which is a combination mixture of sand, clay or other minerals, water, and bitumen, utilizing a hot water separation process developed by Karl Clark in 1920s[25,37,60,61] as shown in Figure 1.3. In the hot water separation process, the oil sands are crushed to make smaller particles, and water at 50−80 °C is added. Bitumen is recovered by flotation called bitumen froth, which consists of 60 wt% bitumen, 30 wt% water, and 10 wt% mineral solids.[25,37,60] A diluent is added to the froth to reduce the viscosity of the oil phase and provide a density difference between oil and inorganic contaminants (e.g. water and solid), called a bitumen froth treatment process.[25,60,62] Diluents are typically an n-paraffin or naphtha, which is a petroleum distillation cut and has carbon numbers in the range of C_5 to C_{12}. The diluted bitumen, water, and inorganic solids separate by gravitational settling and a higher purification of bitumen compared to the bitumen froth is produced, which has impurities of 2-5 wt% water and 0.5-1 wt% solid.[25,37] None

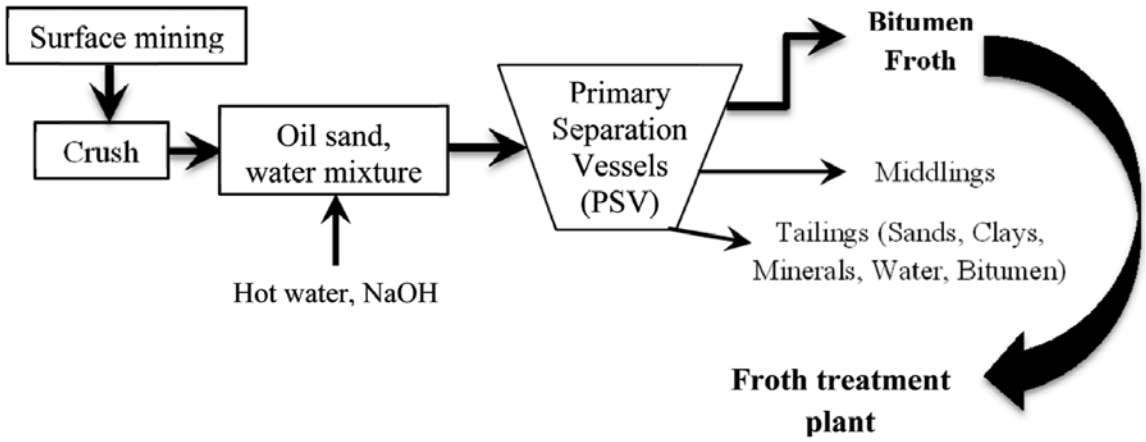

Figure 1.3 Schematic diagram of hot water separation process.[25]

of the previous work has investigated the kinetic precipitation of asphaltenes with the presence of the inorganic solids even though the solids are always present in the production. This investigation leads to a better understanding of the asphaltene aggregation process in systems with inorganic solids and the possible mechanisms for asphaltene precipitation.

1.4 Overview of Chapters

In all previous temperature-reversibility experiments,[11,12,50–52,56] a precipitant was added to aid in destabilizing asphaltenes and/or the effect of experimental time for complete asphaltene precipitation and redissolution was not considered. Reversibility of asphaltenes using temperature-induced aggregation was reinvestigated in this study using a novel experiment that considered the kinetic precipitation of asphaltenes by performing experiments at the equilibrium state and is shown in Chapter 2. Determining whether the asphaltene precipitation process is reversible or not will provide valuable insight to model asphaltene phase behavior. The results could suggest that the thermodynamic or colloidal models better represent the asphaltene behavior. The root cause(s) of the previous results indicating partial reversibility of asphaltene precipitation was also investigated.

In Chapter 3, a combined investigation of asphaltene precipitation and deposition is presented. Asphaltene precipitation was investigated as a function of precipitant types and concentrations. The growth of asphaltene precipitation was also simulated and modeled using a geometric population balance model. Asphaltene deposition was studied using a capillary apparatus by measuring pressure drop inside of the capillary tube. The higher pressure drop indicates the higher occurrence of asphaltene deposition. A relationship between asphaltene aggregation and deposition was explored using Hildebrand solubility parameters. Rather than studying asphaltene precipitation and

deposition independently as was done previously, this study investigated both processes in order to have a better understanding of their relationship.

In Chapter 4, kinetic precipitation of asphaltenes with the presence of inorganic solids in bitumen was investigated. Kinetic precipitation of asphaltenes has previously been investigated with low asphaltene content and without the presence of dispersed solids.[7,21,40,46,63–65] However, bitumen samples, such as Athabasca bitumen, have high asphaltene content and solids are also present. A combined homogeneous aggregation and heterogeneous nucleation model was developed to quantify the rate of asphaltene precipitation under the explored experimental conditions. Characterization of the solids was performed using Scanning Electron Microscopy with Energy Dispersive X-ray Spectroscopy (SEM-EDS). This investigation leads to a better understanding of the asphaltene aggregation process in systems with inorganic solids and provides a simple model that can estimate the rate of asphaltene precipitation under different process conditions. Moreover, this work provides a potential new tool to increase the rate of the often-slow kinetic precipitation of asphaltenes using inorganic solids as nucleation sites to remove unstable asphaltenes.

Chapter 5 discusses the main conclusions and proposed future work.

1.5 References

(1) U.S. Energy Information Administration. *International energy outlook 2016*; 2016.

(2) Miller, R. G.; Sorrell, S. R. *Philos. Trans. A. Math. Phys. Eng. Sci.* **2014**, *372*.

(3) Labban, M. *Space, Oil and Capital*; Routledge: New York, 2008; pp 1–12.

(4) Ahmed, H.; John, R. *Asphaltenes, Heavy Oils, and Petroleomics*; Springer: New York, 2007; pp 617–660.

(5) Cimino, R.; Correra, S.; Bianco, A. D.; Lockhart, T. P. *Asphaltene: Fundamentals*

and Applications; Springer: New York, 1995; pp 97–130.

(6) Yarranton, H. W.; Masliyah, J. H. *AICHE Jounal* **1996**, *42* (12), 3533–3543.

(7) Maqbool, T.; Srikiratiwong, P.; Fogler, H. S. *Energy Fuels* **2011**, *25* (2), 694–700.

(8) Gray, M. R. *Upgrading Petroleum Residues and Heavy Oils*; The University of Alberta Press Ring: Alberta, 2015; pp 1–15.

(9) Speight, J. *The chemistry and technology of petroleum*; CRC Press: New York, 2007; pp 1–60.

(10) Juyal, P.; Ho, V.; Yen, A.; Allenson, S. J. *Energy Fuels* **2012**, *26* (5), 2631–2640.

(11) Peramanu, S.; Singh, C.; Agrawala, M.; Yarranton, H. W. *Energy Fuels* **2001**, *15* (4), 910–917.

(12) Wang, J.; Brower, K.; Buckley, J. *Proc. SPE Int. Symp. Oilf. Chem.* **1999**, 1–7.

(13) Beck, J.; Svrcek, W. Y.; Yarranton, H. W. *Energy Fuels* **2005**, *19* (3), 944–947.

(14) Mullins, O. *SPE J.* **2008**, *13* (1), 48–57.

(15) Tharanivasan, A. K.; Svrcek, W. Y.; Yarranton, H. W.; Taylor, S. D.; Merino-Garcia, D.; Rahimi, P. M. *Energy Fuels* **2009**, *23* (8), 3971–3980.

(16) Mannistu, K. D.; Yarranton, H. W.; Masliyah, J. H. *Energy Fuels* **1997**, *11* (3), 615–622.

(17) Alboudwarej, H.; Akbarzadeh, K.; Beck, J.; Svrcek, W. Y.; Yarranton, H. W. *AIChE J.* **2003**, *49* (11), 2948–2956.

(18) Wiehe, I. a. *Energy Fuels* **2012**, *26* (7), 4004–4016.

(19) Gonzalez, D. L.; Vargas, F. M.; Mahmoodaghdam, E.; Lim, F.; Joshi, N. *Energy Fuels* **2012**, *26* (10), 6218–6227.

(20) Lin, Y.-J.; He, P.; Tavakkoli, M.; Mathew, N. T.; Fatt, Y. Y.; Chai, J. C.; Goharzadeh, A.; Vargas, F. M.; Biswal, S. L. *Langmuir* **2016**, *32* (34), 8729–8734.

(21) Hoepfner, M. P.; Limsakoune, V.; Chuenmeechao, V.; Maqbool, T.; Fogler, H. S. *Energy Fuels* **2013**, *27* (2), 725–735.

(22) Gonzalez, D. L.; Ting, P. D.; Hirasaki, G. J.; Chapman, W. G. *Energy Fuels* **2005**, *19* (4), 1230–1234.

(23) Vargas, F. M.; Gonzalez, D. L.; Hirasaki, G. J.; Chapman, W. G. *Energy Fuels* **2009**, *23* (6), 1140–1146.

(24) Creek, J. *Energy Fuels* **2005**, *19* (4), 1212–1224.

(25) Rao, F.; Liu, Q. *Energy Fuels* **2013**, *27* (12), 7199–7207.

(26) Creek, J. J. L. *Energy Fuels* **2005**, *19* (4), 1212–1224.

(27) Pomerantz, A. E.; Hammond, M. R.; Morrow, A. L.; Mullins, O. C.; Zare, R. N. *Energy Fuels* **2009**, *23* (3), 1162–1168.

(28) Akbarzadeh, K.; Hammami, A.; Kharrat, A.; Zhang, D.; S., A.; Creek, J.; Kabir, S.; Jamaluddin, A.; Marshall, A. G.; Rodgers, R. P.; Mullins, O. C.; Solbakken, T. *Oilf. Rev.* **2007**, No. 2, 22–43.

(29) Zuo, J. Y.; Mullins, O. C.; Dong, C.; Zhang, D. *Nat. Resour.* **2010**, *1*, 19–27.

(30) Hortal, A. R.; Martínez-Haya, B.; Lobato, M. D.; Pedrosa, J. M.; Lago, S. *J. Mass Spectrom.* **2006**, *41* (7), 960–968.

(31) Herod, A. A.; Bartle, K. D.; Kandiyoti, R. *Energy Fuels* **2008**, *22* (6), 4312–4317.

(32) Groenzin, H.; Mullins, O. C. *Energy Fuels* **2000**, *14* (3), 677–684.

(33) Andrews, A. B.; Guerra, R. E.; Mullins, O. C.; Sen, P. N. *J.Phys. Chem* **2006**, *110* (26).

(34) Durand, E.; Clemancey, M.; Lancelin, J. M.; Verstraete, J.; Espinat, D.; Quoineaud, A. A. *Energy Fuels* **2010**, *24* (2), 1051–1062.

(35) Eyssautier, J.; Levitz, P.; Espinat, D.; Jestin, J.; Gummel, J.; Grillo, I.; Barré, L. *J. Phys. Chem. B* **2011**, *115* (21), 6827–6837.

(36) Mullins, O. C.; Sabbah, H.; Pomerantz, A. E.; Andrews, a B.; Ruiz-morales, Y.; Mostow, F.; Mcfarlane, R.; Goual, L.; Lepkowicz, R.; Cooper, T.; Orbulescu, J.; Leblanc, R. M.; Edwards, J.; Zare, R. N.; Barre, L.; Andrews, a B.; Ruiz-morales, Y.; Mostowfi, F.; Mcfarlane, R.; Goual, L.; Lepkowicz, R.; Cooper, T.; Orbulescu, J.; Leblanc, R. M.; Edwards, J.; Zare, R. N. *Energy Fuels* **2012**, *26* (7), 3986−4003.

(37) Mullins, O. C.; Sheu, E. Y.; Hammami, A.; Marshall, A. G. *Asphaltenes, Heavy Oils, and Petroleomics*; Springer: New York, 2007; p 469−488.

(38) Rogel, E.; Rogel, E. *Langmuir* **2004**, *20*, 1003–1012.

(39) Sirota, E. B.; Lin, M. Y. *Energy Fuels* **2007**, *21* (5), 2809–2815.

(40) Maqbool, T.; Balgoa, A. T.; Fogler, H. S. *Energy Fuels* **2009**, *23* (9), 3681–3686.

(41) Mitchell, D. L.; Speight, J. G. *Energy Fuels* **1972**, *52* (2), 149–152.

(42) Wang, J.; Buckley, J. S. *Energy Fuels* **2003**, *17* (7), 1445–1451.

(43) Kraiwattanawong, K.; Fogler, H. S.; Gharfeh, S. G.; Singh, P.; Thomason, W. H.; Chavadej, S. *Energy Fuels* **2007**, *21* (3), 1248–1255.

(44) Wang, J. X.; Buckley, J. S. *Energy Fuels* **2001**, *15* (5), 1004–1012.

(45) Haji-Akbari, N.; Teeraphapkul, P.; Balgoa, A. T.; Fogler, H. S. *Energy Fuels* **2015**, *29* (4), 2190–2196.

(46) Haji-Akbari, N.; Masirisuk, P.; Hoepfner, M. P.; Fogler, H. S. *Energy Fuels* **2013**, *27* (5), 2497–2505.

(47) Hirschberg, A.; DeJong, L. N. J.; Schipper, B. A.; Meijer, J. G. *Soc. Pet. Eng. J.* **1984**, *24* (3), 283–293.

(48) Sandler, S. I. *Chemical, Biochemical, and Engineering Thermodynamics*; John Wiley & Sons, Inc.: New Jersey, 2006; pp 437–597.

(49) Prasnitz, J. M.; Lichtenthaler, R. N.; Gomes de Azevedo, E. *Chemical, Biochemical, and Engineering Thermodynamics*; Prentice Hall PTR: New Jersey, 1999; pp 421–439.

(50) Abedini, A.; Ashoori, S.; Torabi, F. *Fluid Phase Equilib.* **2011**, *308* (1–2), 129–134.

(51) Ahmadi, Y.; Kharrat, R.; Hashemi, A.; Bahrami, P.; Mahdavi, S. *Pet. Sci. Technol.* **2014**, *32* (18), 2263–2273.

(52) Abedini, A.; Ashoori, S.; Torabi, F.; Saki, Y.; Dinarvand, N. *J. Pet. Sci. Eng.* **2011**, *78* (2), 316–320.

(53) Hammami, A.; Phelps, C. H.; Monger-McClure, T.; Little, T. M. *Energy Fuels* **2000**, *14* (1), 14–18.

(54) Clarke, P. F.; Pruden, B. B. 47th Annual Technical Meeting of The Petroleum Society; 1996; pp 96–112.

(55) Ramos, A. C. S.; Delgado, C. C.; Mohamed, R. S.; Almeida, V. R.; Loh, W. *the Fifth Latin Amencan and Caribbean Petroleum Engineering Conference and Exhibition*; 1997; pp 1–5.

(56) Andersen, S. I.; Stenbya, E. I. *Fuel Sci. Technol. Int.* **1996**, *14* (1–2), 261–287.

(57) Mohammadi, S.; Rashidi, F.; Mousavi-Dehghani, S. A.; Ghazanfari, M. H. *J. Chem. Eng. Data* **2015**, *60* (9), 2646–2654.

(58) Mohameda, R. S.; Lohb, W.; Ramos, A. C. S.; Delgado, C. C.; Almeida, V. R. *Pet. Sci. Technol.* **1999**, *17* (7–8), 877–896.

(59) Haji-Akbari, N.; Teeraphapkul, P.; Fogler, H. S. *Energy Fuels* **2014**, *28* (2), 909–919.

(60) Yang, X.; Czarnecki, J. *Colloids Surfaces A Physicochem. Eng. Asp.* **2002**, *211* (2–3), 213–222.

(61) Clark, K. A.; Pasternack, D. S. *Ind. Eng. Chem.* **1932**, *24* (12), 1410-14–16.

(62) Yang, X.; Hamza, H.; Czarnecki, J. *Energy Fuels* **2004**, *18* (3), 770–777.

(63) Chaisoontornyotin, W.; Haji-Akbari, N.; Fogler, H. S.; Hoepfner, M. P. *Energy Fuels* **2016**, *30* (3), 1979–1986.

(64) Chaisoontornyotin, W.; Bingham, A. W.; Hoepfner, M. P. *Energy Fuels* **2017**, *31* (4), 3392–3398.

(65) Maqbool, T.; Raha, S.; Hoepfner, M. P.; Fogler, H. S. *Energy Fuels* **2011**, *25* (4), 1585–1596.

CHAPTER 2

REVERSIBILITY OF ASPHALTENE PRECIPITATION USING TEMPERATURE-INDUCED AGGREGATION

Reprinted with permission from Chaisoontornyotin, W.; Bingham, A. W.; Hoepfner, M. P. Energy & Fuels 2017, 31 (4), 3392–3398.

energy&fuels

Article

pubs.acs.org/EF

Reversibility of Asphaltene Precipitation Using Temperature-Induced Aggregation

Wattana Chaisoontornyotin, Austin W. Bingham, and Michael P. Hoepfner*

Department of Chemical Engineering, University of Utah, Salt Lake City, Utah 84112, United States

ABSTRACT: In this work, kinetic asphaltene precipitation was investigated using temperature fluctuations. Asphaltene precipitation was previously identified as a fully reversible process by altering the solution pressure or composition but only partially reversible using temperature changes. Slow kinetic asphaltene precipitation plays a critical role in the accurate monitoring of asphaltene precipitation, and previous reversibility studies need to be revisited in light of this phenomenon. Previous studies used a combination of precipitant addition and temperature changes to conclude that precipitated asphaltenes do not fully redissolve when the mixture temperature is changed. Modeling results reveal that precipitated asphaltenes should not be expected to redissolve, regardless of the magnitude of temperature changes, after a precipitant (e.g., dodecane) is added to the mixture. Consequently, this study was designed to isolate the influence of slow kinetics, precipitant addition, and temperature changes on the solubility and reversibility of asphaltene precipitation. Temperature cycling experiments were performed to investigate the reversibility of asphaltene precipitation and revealed that the process is fully reversible with temperature changes. This finding reinforces that, for the system in this study, asphaltene phase behavior is controlled by equilibrium thermodynamics and not a colloid stabilization model.

INTRODUCTION

Crude oil and bitumen are complex mixtures of hydrocarbons that are commonly categorized into saturates, aromatics, resins, and asphaltenes, called SARA fractions.[1−5] Asphaltenes represent the heaviest oil fraction, and they are defined as the material that is soluble in aromatic solvents [e.g., toluene and 1-methylnaphthalene (1-MN)] and insoluble in *n*-alkanes (e.g., *n*-heptane and *n*-decane).[2,4,6−16] Asphaltenes typically consist of a polyaromatic core with various alkyl side chains and contain heteroatoms (N, S, and O) and trace metals (e.g., Ni, V, and Fe).[1] During oil production, transportation, and processing, changes in pressure, temperature, and composition can result in the destabilization of asphaltenes.[4,8,9,13,17] Destabilized asphaltenes can precipitate and deposit in processing and refining equipment and also stabilize water-in-oil emulsions.[1,4,9,13,18] Asphaltene fouling issues ultimately lead to decreases in oil productivity, production downtime, and downstream issues, such as fouling in heat exchangers.[1,4,9,13] In this study, "aggregation" describes the asphaltene size transition from the nanometer to micrometer size and "precipitation" refers to the entire process of asphaltenes transitioning from stable nanoaggregates/clusters to unstable micrometer-sized flocs.[19]

Previous studies have shown that asphaltene precipitation is a kinetic aggregation process and the detection of precipitated asphaltenes can take weeks or months at sufficiently low precipitation concentrations.[4,19−23] At higher precipitant concentrations, asphaltene destabilization may be detected over shorter experimental durations but an accurate measurement of the asphaltene solubility may require additional time.[4,19,21] Previous work on asphaltene stability or phase envelopes should be revisited, because asphaltenes may be unstable and precipitating under conditions where they were previously thought to be stable or fully soluble.

Reversibility is a requirement for the application of equilibrium thermodynamics to predict the phase behavior of mixtures.[24,25] Determining whether the asphaltene precipitation process is reversible or not will provide valuable insight into determining whether colloidal[2,26−32] or solubility[33−36] models are appropriate to model asphaltene phase behavior. The colloidal model is based on the concept that asphaltenes are stabilized by resins, maltenes, or other asphaltene fractions and that, once the asphaltenes are destabilized, the precipitation is irreversible.[2,26,27,37] Solubility approaches use thermodynamic phase behavior models to describe the solution behavior of asphaltenes. If asphaltene precipitation is a reversible process, it suggests that solubility models are more suitable to investigate and model asphaltene precipitation.

Reversibility of asphaltene precipitation has been investigated using changes in pressure, composition, and temperature to destabilize asphaltenes.[1,7,8,36,38−45] Hammami et al.[41] investigated the reversibility of asphaltene precipitation and concluded that asphaltene precipitation using pressure depletion is a reversible process. In this study, a solids detection system was used to measure light transmittance through a solution in a pressure−volume−temperature (*PVT*) cell. Below the onset pressure of asphaltene precipitation, light transmittance decreased as a result of the presence of precipitated asphaltenes and, subsequently, increased back to the original state after the system was pressurized back above the onset pressure. This experiment and others[36,38−40,44] demonstrate the reversible process of asphaltene precipitation using pressure-induced aggregation.

Special Issue: 17th International Conference on Petroleum Phase Behavior and Fouling

Received: September 15, 2016
Revised: January 10, 2017
Published: January 12, 2017

DOI: 10.1021/acs.energyfuels.6b02344
Energy Fuels 2017, 31, 3392−3398

Optical microscopy was used in the study of Ramos et al.[43] and Mohamed et al.[45] to investigate the thermodynamic reversibility of asphaltene precipitation as a result of changes in composition by adding and removing a precipitant (e.g., *n*-heptane). The images revealed that the precipitated asphaltenes dissolved upon *n*-heptane removal to demonstrate reversibility, and this study is in agreement with other similar investigations.[8,9,38,40,42] Previous studies have also found that the redissolution process can be time-dependent.[41,42]

The reversibility of asphaltene precipitation as a result of changes in the temperature was also previously investigated using a variety of experimental approaches, such as optical microscopy, gravitational methods, and a flow loop system.[7,8,38−40] The previous work,[7,8,38−40] investigating the reversibility of asphaltene precipitation with temperature changes, all started their experimental procedure by adding a precipitant into a crude oil. The precipitant concentrations were approximately 65−90 vol %.[8,38,40] The temperature of the solution was then increased or decreased before returning back to the initial value. Reversibility in asphaltene precipitation was not observed in these previous investigations, and the experimental asphaltene precipitation detection measurements differed between the initial and final states. For example, Peramanu et al.[8] used the pressure drop in a flow loop system, and Abedini et al.[38,40] measured the mass of precipitated asphaltenes gravimetrically. In both cases, the initial pressure drop and masses were not the same values after performing a temperature cycle. Despite the different measurement approaches, the same conclusion of partial asphaltene precipitation reversibility was reached.

The results of previous work lead to similar conclusions that, using pressure and composition-induced aggregation, asphaltene precipitation is a reversible process but only partially reversible using temperature changes.[1,7,8,36,38−45] However, in all previous temperature-reversibility experiments,[7,8,38−40] a precipitant was added to aid in destabilizing asphaltenes and/or the effect of experimental time for complete asphaltene precipitation and redissolution was not considered. Adding a precipitant to conveniently observe asphaltene precipitation, in addition to changing the temperature, represents two simultaneous (and competing) asphaltene destabilizing mechanisms. Therefore, to isolate the influence of the temperature on asphaltene stability, composition-induced aggregation effects must be considered and eliminated. Ideally, this temperature-reversibility study would consist of monitoring asphaltene precipitation as a function of the time and temperature only, without adding a precipitant. However, the temperature needed to destabilize asphaltenes would vary based on asphaltene origin and solvent. Adding a precipitant is a means to ensure that the phase transition point for asphaltenes as a function of the temperature is practical and safe for a laboratory setting. Thus, both composition and temperature act as destabilizing agents in this study and previous work.[7,8,38−40] However, the composition-induced aggregation effect is isolated, in this study, and removed such that the asphaltene precipitation from only the change of the temperature can be achieved.

One common and relatively straightforward approach to investigate the phase behavior of asphaltene is a Flory−Huggins-type model. Painter et al.[46−48] developed an association model modified from a Flory−Huggins approach to include the free volume difference between asphaltenes and solvent using an effective interaction parameter, χ_{eff}.[47] The effective interaction parameter is used to represent the asphaltene stability in the solution as a first approximation of the asphaltene phase behavior. As an approximation, it is assumed that higher interaction parameters indicate lower solubility of asphaltenes.[46,47] In this study, the previous conclusions of partial reversibility of asphaltene precipitation with respect to temperature-induced aggregation are investigated using the effective interaction parameter.

One of the primary objectives of this work is to investigate the root cause(s) of the previous results indicating partial reversibility of asphaltene precipitation. Additionally, this study aims to determine whether the consideration of kinetic asphaltene precipitation can demonstrate that asphaltene precipitation is a fully reversible process. A phase diagram for asphaltene stability as a function of the temperature was also developed and presented, along with an estimation of the effective interaction parameter between asphaltene aggregates and solvent. Furthermore, validating that temperature changes can both precipitate and redissolve asphaltenes opens new strategies for performing and investigating asphaltene behavior. Temperature changes are, in general, easier to control in the laboratory compared to pressure or compositional differences at atmospheric pressure conditions.

■ EXPERIMENTAL METHODS

Material and Asphaltene Extraction. All liquid diluents (e.g., 1-MN, toluene, dodecane, and *n*-heptane) were high-performance liquid chromatography (HPLC)-grade and supplied from Fisher Scientific. Asphaltenes were extracted from an Athabasca oil sands bitumen source. To extract the solid asphaltenes, bitumen was heated to 60 °C, mixed with *n*-heptane in a 20:1 by weight ratio, and homogenized for 24 h with a magnetic stirrer. After 24 h, no bitumen adhered on the sides or bottom of the container, suggesting that the solution was well-mixed. Asphaltenes were then separated using an Eppendorf 5430 R centrifuge at a relative centrifugal force (RCF) of 3000*g* for 10 min. The supernatant was decanted, and the cake was transferred to a 2.5 in. diameter ceramic thimble for washing, to remove residual oil and debris, in heptane using a Soxhlet extractor for 24 h. The thimble was placed in a vacuum oven with a vacuum gauge pressure of 7.4 psi (4.9 psi absolute pressure) at 75 °C for 24 h, to allow for any residual heptane to evaporate. After the asphaltenes were fully dried, the thimble and asphaltenes were placed back in the Soxhlet, this time to be washed with toluene for 24 h to remove any residual inorganic solids. Residual toluene was removed by forced convection, and the solid asphaltenes were dried in a vacuum oven (7.4 psi gauge) at 75 °C for 24 h or until consecutive weights (at least 2 h of separation) were within ±0.1 g. Extracted asphaltenes were used to mix with a solvent to obtain a solution called a model oil.

Phase Diagram. Solutions of 1 vol % (1.2 wt %) asphaltene in 1-MN were previously used to generate an asphaltene solubility phase diagram,[35] and in this study, an analogous same system was also prepared. The asphaltenes in 1-MN solution, called the model oil, and a separate container of dodecane were each preheated to 80 °C. The asphaltene solution and dodecane were mixed together to obtained desired concentrations (vol %) at 80 °C. The solution was kept at 80 °C for 2 h; at which point, samples were taken and, subsequently, observed under an optical microscope to confirm that all asphaltenes were dissolved. The temperature was then decreased in 10 °C intervals, whereby each change in the temperature was held constant for 45 min. If precipitated asphaltenes were observed at a given temperature interval, via visual inspection by inverting the storage vial, the temperature was recorded and identified as the precipitation temperature.

Model of the Interaction Parameter. Painter et al.[46−48] developed an association model that considered the association of asphaltene molecules to form nanoaggregates[48] and the free volume difference between asphaltenes and solvent[47] using a Flory−Huggins equation and an effective interaction parameter, χ_{eff}, which is assumed

DOI: 10.1021/acs.energyfuels.6b02344
Energy Fuels 2017, 31, 3392−3398

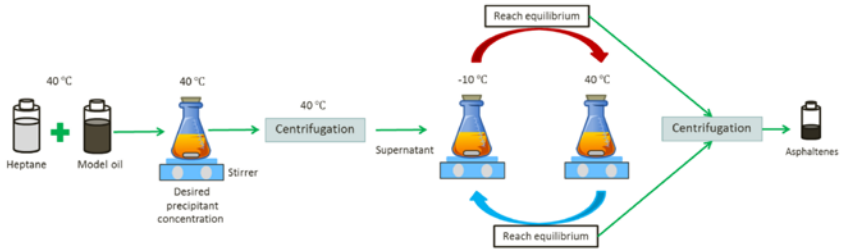

Figure 1. Schematic diagram of the temperature cycling experiment.

to be composition-independent.[46,47] The entropic term considers the free volume effect, and the enthalpic term considers non-specific interactions between asphaltenes and solvent using the solubility parameter, as shown in eq 1

$$\chi_{\text{eff}} = \chi_s + \chi_H = \chi^{fv} + \frac{V_s}{RT}(\delta_a - \delta_s)^2 \quad (1)$$

where χ_{eff} is the effective interaction parameter, χ_s is the entropic component interaction parameter, χ_H is the enthalpy component interaction parameter, χ^{fv} is the interaction parameter for the free volume effect, V_s is the molecular or specific volume (cm^3/mol), R is the universal gas constant (8.314×10^6 Pa cm^3 mol^{-1} K^{-1}), T is the temperature (K), and δ_a and δ_s are the solubility parameters of asphaltenes and solvent, respectively ($Pa^{0.5}$). The free volume effect between asphaltenes and solvent, χ^{fv}, can be estimated using the molar volume of the solvent.[47] For compact, rigid, and nonpolar molecules, such as toluene and 1-MN, χ^{fv} can be calculated by $\chi^{fv} = 0.466 - 0.00327V_s$, and for flexible and nonpolar molecules, such as heptane and *n*-paraffins, χ^{fv} can be calculated using $\chi^{fv} = 0.82 - 0.00462V_s - 0.0000133V_s^2$.[47] A volumetric average of the rigid and flexible contributions to χ^{fv} was used in this study to model the 1-MN–dodecane mixture as a pseudo-component solvent. It was assumed that, for χ_s calculation, V_s is independent of the temperature and, for χ_H calculation, V_s, δ_s, and δ_a are a function of the temperature. The molar volume and solubility parameter $\{\delta_s = [(\Delta H^{vap} - RT)/V_s]^{0.5}\}$ as a function of the temperature were calculated from published data.[49−53] In this study, asphaltenes were extracted from the same source with the same precipitant and only the temperature was varied. Thus, the temperature-dependent asphaltene solubility parameter was calculated using $\delta_a = 20.04[1 - 1.07 \times 10^{-3}(T - 273.15)] \times 10^3$.[54] The interaction parameter between asphaltenes and solvents is used in this study as an approximation for the asphaltene stability and solubility to investigate potential causal factors, leading to the previous conclusions that asphaltenes are partially reversible under temperature-induced aggregation.[7,8,38−40]

Asphaltene Solubility. A precipitant, *n*-heptane, and a model oil mixture of 3 vol % (4.3 wt %) asphaltenes in toluene were heated or cooled (depending upon the experimental conditions) in separate glass vials until reaching the desired temperature of −10, 20, or 40 °C. The temperature range was selected on the basis of the minimum and maximum operating temperatures of the centrifuge. Following the procedure by Chaisoontornyotin et al.,[19] heptane was then added to the model oil to obtain the desired concentration (vol %). An Isotemp 5150 R28 chiller bath was used to maintain the temperature of the −10 °C experiments using a jacketed beaker. An IKA RT15 multi-position hot stir plate was used for the experiments at 20 and 40 °C. After the precipitant and model oil were combined, the solution was allowed to stir continuously at 350 rpm using either the multi-position hot stir plate or the jacketed beaker mounted to a stir plate. To determine the quantity of precipitated asphaltenes, two 1.5 mL samples were loaded into 1.5 mL microcentrifuge tubes and centrifuged for 10 min at 14 000 rpm (19283*g*) in an Eppendorf 5430 R centrifuge set to the experimental temperature. The supernatant was carefully decanted so as not to disturb the cake. The cake was washed with heptane and dried in the oven. Additional details of the washing step can be found elsewhere.[19] The mass fraction of precipitated asphaltenes as a function of the time and temperature was measured.

Temperature Cycling. A precipitant, heptane, and model oil were heated in separate containers to 40 °C, as shown in Figure 1. Heptane at 40 °C was then transferred to a glass vial containing the model oil to achieve the desired precipitant concentration. The solution was then placed on an IKA RT15 multi-position hot stir plate set to 40 °C, where the asphaltenes then precipitated for a time until, as indicated by the previously conducted solubility experiments, the rate of precipitation was negligible. After reaching equilibrium, the entire solution was centrifuged to remove the precipitated asphaltenes. Because of the need to centrifuge large volumes of solution, the centrifuge was set to 5000 rpm (2935*g*) rather than 14 000 rpm at 40 °C for 10 min. Note that the mass of precipitated asphaltenes using 5000 and 14 000 rpm for 10 min was measured, and no appreciable difference in the mass of precipitated asphaltenes was observed. Upon centrifugation of the model oil and heptane mixture, the supernatant was decanted and transferred to a new glass vial, placed in a jacketed beaker, chilled to −10 °C, and mounted on top of the magnetic stir plate. The mixture was stirred until the rate of precipitation was negligible, as determined from the results of the Asphaltene Solubility section; at which point, two 1.5 mL samples were taken, centrifuged, decanted, washed with heptane, and dried in the oven. The centrifugation conditions were 10 min at 14 000 rpm (19283*g*). Two more 1.5 mL samples were taken at least 6 h later, following the same procedure. Upon taking the four samples at the −10 °C condition, the mixture was placed on the 40 °C hot plate and allowed to reach equilibrium. Then, two 1.5 mL samples were taken, centrifuged, decanted, washed, and dried, followed 6 h later by two more samples. The eight samples taken at −10 and 40 °C comprise one full temperature cycle. Three full cycles were conducted for each temperature cycling experiment.

■ RESULTS AND DISCUSSION

Precipitation temperatures of 1 vol % asphaltenes in 1-MN at various dodecane concentrations are displayed in Figure 2. A decrease in the temperature resulted in the precipitation of asphaltenes, and higher dodecane concentrations resulted in higher precipitation temperatures. If this process is thermodynamically reversible, the precipitated asphaltenes will dissolve when the temperature is increased above the precipitation temperature. However, after raising the temperature, the photographs of the 20 and 28 vol % 1-MN solutions in Figure 2 show that precipitated asphaltenes adhered on the sides or bottom of the container. This result reveals that complete dissolution of asphaltenes was not observed after raising the temperature and is in agreement with previous results.[7,8,38−40] Previous work used this observation to conclude that

DOI: 10.1021/acs.energyfuels.6b02344
Energy Fuels 2017, 31, 3392−3398

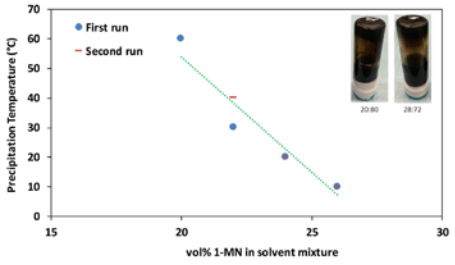

Figure 2. Precipitation temperatures of a 1 vol % asphaltene in 1-MN at various dodecane concentrations. Experiments were performed twice, indicated as the first and second runs.

asphaltene precipitation is only partial reversibility with destabilization induced by temperature changes. However, this experiment and similar previous experiments did not consider the effect of slow precipitation kinetics following the addition of a precipitant to the solution. It is possible that the initial addition of a precipitant destabilized asphaltenes, and this instability was unnoticed as a result of long detection times. Consequently, the initial state of the system at an elevated temperature was never actually representative of a stable mixture, and reheating a cooled mixture would not force asphaltenes to dissolve. Thus, it was hypothesized that the consistent conclusions regarding the partial reversibility of asphaltenes is influenced by kinetic, composition, and temperature effects and isolation of these individual influences is necessary.

To investigate the cause of partial reversibility of asphaltene precipitation, the effective interaction parameter, χ_{eff}, was estimated as a function of the temperature and dodecane concentration and displayed in Figure 3. The results of the

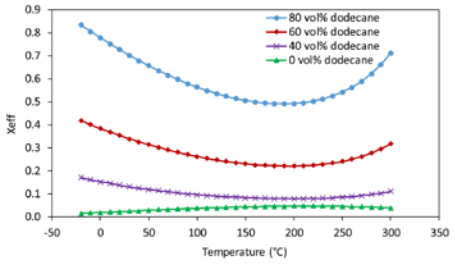

Figure 3. Interaction parameter using the model by Painter et al.[46−48] for asphaltenes in various dodecane concentrations in 1-MN as a function of the temperature.

dodecane concentration at 0 and between 40 and 80 vol % were shown because previous studies[7,8,38−40] used 65−90 vol % precipitant concentrations. The results show that χ_{eff} increases with higher dodecane concentrations. After >40 vol % dodecane is added to a solution of asphaltenes and 1-MN, the effective interaction parameter does not decrease to the value at 0 vol % dodecane, regardless of the magnitude of the temperature increase. This analysis is intended to demonstrate approximate trends that, after a precipitant is added, asphaltenes behave differently in solvent−precipitant mixtures compared to pure solvent. It is not necessarily appropriate to assume that a temperature increase with a precipitant is representative of a system with no precipitant added. Previous work on asphaltene reversibility with temperature changes[7,8,38−40] were likely influenced heavily by the change in composition when adding a precipitant and cannot be used to definitively conclude that asphaltene precipitation is partially reversible for temperature changes. It can be also observed that the interaction parameter from 0 and 100 °C for 40, 60, and 80 vol % dodecane decreases by 37, 32, and 28%, respectively. These results show that, at lower precipitant concentrations, a change in the temperature can have a larger relative influence on the interaction parameter. This finding matches previous experimental observations that demonstrate a larger difference in asphaltene solubility at different temperatures using lower precipitant concentrations.[4] It is important to note that the interaction parameter can be used to determine the solubility of asphaltenes, but to fully understand the relation between the interaction parameter and solubility, a complete thermodynamic model is needed. Figure 3 is presented for illustrative purposes and is not comprehensive.

The instantaneous onset point of the toluene model oil was between 46 and 48 vol % heptane concentration, as determined by optical microscopy. Precipitant concentrations of 40 and 45 vol % heptane in model oil and the temperature range from −10 to 40 °C were used for further studies because they were a compromise between the time required to reach the equilibrium solubility and the solubility being sensitive to moderate temperature changes. The percent mass of precipitated asphaltenes as a function of the time and temperature for 40 and 45 vol % heptane in a 3 vol % asphaltene in toluene model oil solution is presented in Figures 4 and 5, respectively. The results from both Figures 4 and 5 display a clear trend of decreasing asphaltene solubility as the temperature is lowered. Additionally, the time to reach equilibrium or equilibration time for a given precipitant concentration and temperature was also obtained from these figures as the earliest measured data point where the precipitated mass remains approximately constant. The equilibrium precipitated mass is then obtained by averaging the last few data that provided a constant mass of precipitated asphaltenes. The equilibration time is used to design the temperature cycling experiments to determine the appropriate waiting time after changing the temperature before taking samples. Figure 4 shows that the equilibration time is approximately 50, 120, and 180 h for temperature conditions of 40, 20, and −10 °C, respectively. Figure 5 indicates that equilibration for the −10 and 40 °C samples is reached in approximately 20−25 h, whereas the 20 °C samples appear to have taken somewhat longer to reach equilibrium, about 60 h. The trend of an increasing equilibration time with a decreasing temperature is not consistent between Figures 4 and 5. However, multiple factors influence this equilibration time, including solution viscosity, asphaltene morphology, and solvation strength. Competing effects are difficult to isolate without a more detailed modeling investigation, which is outside of the scope of this study. Moreover, it can be observed that the equilibration time for the precipitated asphaltenes was faster and the kinetic precipitation effect of asphaltenes is less pronounced at higher precipitant concentrations, in agreement with numerous previous studies.[4,19,21]

DOI: 10.1021/acs.energyfuels.6b02344
Energy Fuels 2017, 31, 3392−3398

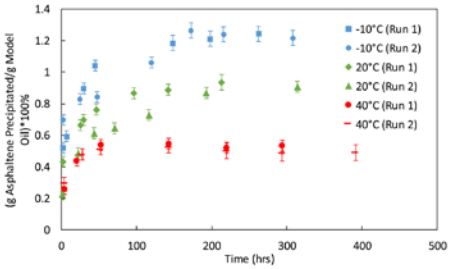

Figure 4. Mass percentage of precipitated asphaltenes as a function of the time for 40 vol % heptane in the 3 vol % asphaltene in toluene model oil.

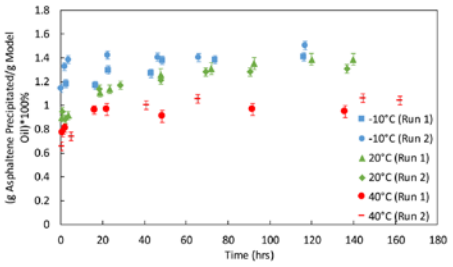

Figure 5. Mass percentage of precipitated asphaltenes as a function of the time for 45 vol % heptane in the 3 vol % asphaltene in toluene model oil.

The equilibrium values for the percent mass of precipitated asphaltenes from the toluene model oil as a function of the temperature and precipitant concentration are plotted in Figure 6. The mass of precipitated asphaltenes at a high temperature was lower compared to the value at a low temperature, in agreement with previous work.[4] Furthermore, for a given temperature change, systems with a lower precipitant concentration exhibit a larger change in asphaltene solubility as a function of the temperature. This result agrees with the

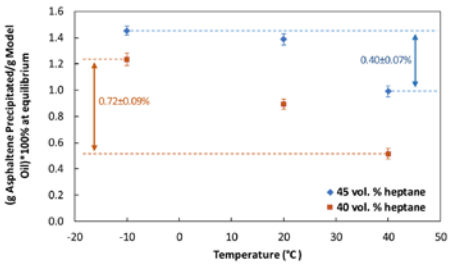

Figure 6. Mass percentage of precipitated asphaltenes at equilibrium as a function of the temperature at 40 and 45 vol % heptane. Dashed lines show the difference in percent mass at the temperature extremes, −10 and 40 °C.

interaction parameter analysis in Figure 3, where a change of the temperature at lower precipitant concentrations results in a larger relative change in the interaction parameter compared to higher precipitant concentrations.

To perform the temperature cycling experiments efficiently, the precipitation equilibration time as well as the mass of precipitated asphaltenes at equilibrium needed to be considered. Before taking samples in the temperature cycling experiments, the solution must reach equilibrium at 40 °C, be centrifuged to remove precipitated asphaltenes, cooled to −10 °C, and allowed to reach equilibrium, as determined by the asphaltene solubility experiments (Figures 4 and 5). This procedure of removing the asphaltenes at 40 °C effectively isolates the composition and temperature effects on solubility. Furthermore, only sampling after the solution has reached equilibrium accounts for the slow precipitation kinetics of asphaltenes. From the asphaltene solubility results, it was determined that suitable precipitant concentrations should be in the range of 40−45 vol % to conduct practical laboratory experiments. In comparison of Figures 4 and 5, it is clear that an increase in the precipitant concentration decreases the difference in percent mass of precipitated asphaltenes between −10 and 40 °C compared to lower precipitant concentrations. Thus, both the 40 and 45 vol % systems have temporally reasonable kinetics and sufficiently different solubilities at the chosen temperatures of −10 and 40 °C for accurate experimental measurements.

The percent mass of precipitated asphaltene for the 45 and 40 vol % heptane systems in the temperature cycling experiments is shown in Figures 7 and 8, respectively. Precipitated asphaltene at 40 °C were removed at the start of the experiment; consequently, the percent mass of precipitated asphaltenes should be 0% at the elevated temperature. The kinetic precipitation of asphaltenes at 40 °C is included at the early times in Figures 7 and 8 to highlight the importance of the slow kinetics, but these experiments were not repeated during the temperature cycling experiments. The results show that, after removing the asphaltenes precipitated by heptane addition at the elevated temperature, the percent mass of precipitated asphaltenes cycled between 0.90 ± 0.18 and 0.02 ± 0.05% at −10 and 40 °C, respectively, for the 45 vol % heptane system (Figure 7). For the 40 vol % heptane system, the percent mass was cycled between 0.91 ± 0.13 and 0.10 ± 0.05% at −10 and 40 °C, respectively (Figure 8). The results reveal that asphaltene precipitation is fully reversible at 45 vol % heptane because, at the high-temperature condition in Figure 7 (45 vol % heptane), the asphaltenes fully redissolve over many temperature cycle iterations. However, as shown in Figure 8, small quantities of precipitated asphaltenes were detected at 40 °C in the 40 vol % heptane system. Slow redissolution kinetics were suspected as the cause of the detected undissolved asphaltenes. To test this hypothesis, additional experiments were performed to allow for longer redissolution times (1 week) in the 40 vol % precipitant system. These experiments gave an average percent mass of precipitated asphaltenes at 40 °C of 0.05 ± 0.04% after waiting 1 week. These results show that, while still not returning to 0%, the longer redissolution times allow for additional asphaltene to dissolve and we expect the 40 vol % system to be reversible, provided that the lengthy kinetics of redissolution are taken into account. The results of slower kinetic redissolution compared to precipitation are in a good agreement with previous work.[41] Moreover, it can be seen that the kinetic redissolution for 40 vol % heptane was slower

DOI: 10.1021/acs.energyfuels.6b02344
Energy Fuels 2017, 31, 3392−3398

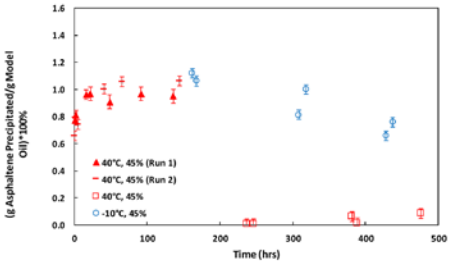

Figure 7. Mass percentage of precipitated asphaltene for 45 vol % heptane from previous runs (1 and 2) to show the kinetics involved in asphaltene precipitation (filled markers) at 40 °C. The mass percentage of precipitated asphaltenes in the temperature cycling experiments (unfilled markers) are also shown at the temperature extremes investigated, −10 °C (unfilled blue boxes) and 40 °C (unfilled red boxes), showing asphaltene reversibility.

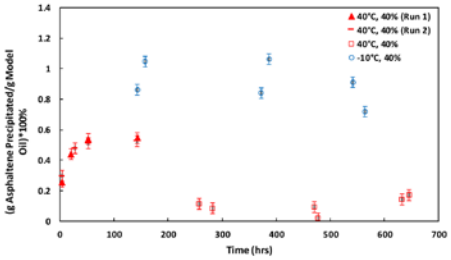

Figure 8. Mass percentage of precipitated asphaltene for 40 vol % heptane from previous runs (1 and 2) to show the kinetics involved in asphaltene precipitation (filled markers) at 40 °C. The mass percentage of precipitated asphaltenes in the temperature cycling experiments (unfilled markers) are also shown at the temperature extremes investigated, −10 °C (unfilled blue circles) and 40 °C (unfilled red circles), showing asphaltene reversibility.

than that for 45 vol % heptane, and further investigation is recommended to investigate this behavior. Another question was whether precipitated asphaltenes that were removed at the beginning of the temperature cycling experiments were responsible for the irreversible precipitation/dissolution behavior in previous work. The answer to this question depends upon whether asphaltene subfractions are expected to behave differently with changes in the temperature or not. When the experiments were performed at two heptane concentrations, 40 and 45 vol % heptane, the experiments tested for the behavior of two asphaltene subfractions. A portion of the asphaltenes precipitated at 45 vol % heptane was soluble in the asphaltene subfraction in the 40 vol % heptane experiments. The results of the temperature cycling experiments using the two subfractions are in a good agreement that asphaltene precipitation is reversible. Not all subfractions were tested in this study as a result of slow kinetic precipitation/dissolution limitations; however, we anticipate that asphaltene precipitation will be reversible for the untested asphaltenic material.

An interesting observation is that the difference in solubility of asphaltenes between 0 and 40 °C in the temperature cycling experiments and the asphaltene solubility experiments is not the same. Figure 6 demonstrates differences in solubility between the extreme temperatures of 0.72 ± 0.09 and 0.40 ± 0.07% for 40 and 45% heptane, respectively; however, in the temperature cycling experiments, differences of 0.81 ± 0.18 and 0.88 ± 0.23% were observed between the two temperatures, 0 and 40 °C, respectively. The temperature cycling experiments involved removing a fraction of the asphaltenes from the model oil mixture, which alters the overall composition of the asphaltene fraction. This observation does not alter the overall conclusion that the system is a thermodynamically reversible system; however, it does highlight the complex interactions that occur within the asphaltene fraction. Furthermore, because the temperature cycling experiments were performed at two different heptane concentrations, different fractions of asphaltenes were removed for each set of experiments yet the end result is the same. Consequently, we believe that the observation of temperature reversibility will hold true for all asphaltene types.

■ CONCLUSION

The results from the experiments performed in this study show that asphaltene precipitation is reversible when using temperature fluctuations as the destabilizing mechanism. Previous work that suggested partial reversibility via temperature-induced aggregation did not consider the long kinetics of asphaltene precipitation. This study, when combined with previous work, reveals that asphaltene precipitation is reversible through all three common destabilizing methodologies: temperature, pressure, and composition changes. This finding is an important result, because the temperature is often an easy experimental parameter to manipulate in the laboratory at atmospheric pressure conditions. These findings suggest that, for the system in this study, a solubility modeling approach is more suitable than a colloid stabilization model to understand asphaltene phase behavior. Consequently, provided that accurate and sufficient experimental characterization is performed, along with a theoretical thermodynamic model, the phase behavior of asphaltenes can be predicted using multicomponent equilibrium thermodynamics.

■ AUTHOR INFORMATION

Corresponding Author

*E-mail: michael.hoepfner@utah.edu.

ORCID

Wattana Chaisoontornyotin: 0000-0003-1202-6702

Notes

The authors declare no competing financial interest.

■ ACKNOWLEDGMENTS

The authors thanks Yuan Yang for helpful discussion and suggestions.

■ REFERENCES

(1) Hammami, A.; Ratulowski, J. Precipitation and Deposition of Asphaltenes in Production Systems: A Flow Assurance Overview. In *Asphaltenes, Heavy Oils, and Petroleomics*; Mullins, O. C., Sheu, E. Y., Hammami, A., Marshall, A. G., Eds.; Springer: New York, 2007; pp 617−660, DOI: 10.1007/0-387-68903-6_23.

(2) Cimino, R.; Correra, S.; Del Bianco, A.; Lockhart, T. P. Solubility and Phase Behavior of Asphaltenes in Hydrocarbon Media. In *Asphaltene: Fundamentals amd Applications*; Sheu, E. Y., Mullins, O. C.,

DOI: 10.1021/acs.energyfuels.6b02344
Energy Fuels 2017, 31, 3392−3398

Eds.; Springer: Boston, MA, 1995; pp 97−130, DOI: 10.1007/978-1-4757-9293-5_3.
(3) Yarranton, H. W.; Masliyah, J. H. *AIChE J.* **1996**, *42* (12), 3533−3543.
(4) Maqbool, T.; Srikiratiwong, P.; Fogler, H. S. *Energy Fuels* **2011**, *25* (2), 694−700.
(5) Gray, M. R. *Upgrading Petroleum Residues and Heavy Oils*; CRC Press (Taylor & Francis Group): Boca Raton, FL, 2015.
(6) Juyal, P.; Ho, V.; Yen, A.; Allenson, S. J. *Energy Fuels* **2012**, *26* (5), 2631−2640.
(7) Wang, J.; Brower, K.; Buckley, J. Advances in Observation of Asphaltene Destabilization. *Proceedings of the SPE International Symposium on Oilfield Chemistry*; Houston, TX, Feb 16−19, 1999; pp 1−7, DOI: 10.2118/50745-MS.
(8) Peramanu, S.; Singh, C.; Agrawala, M.; Yarranton, H. W. *Energy Fuels* **2001**, *15* (4), 910−917.
(9) Beck, J.; Svrcek, W. Y.; Yarranton, H. W. *Energy Fuels* **2005**, *19* (3), 944−947.
(10) Mullins, O. *SPE J.* **2008**, *13* (1), 48−57.
(11) Tharanivasan, A. K.; Svrcek, W. Y.; Yarranton, H. W.; Taylor, S. D.; Merino-Garcia, D.; Rahimi, P. M. *Energy Fuels* **2009**, *23* (8), 3971−3980.
(12) Mannistu, K. D.; Yarranton, H. W.; Masliyah, J. H. *Energy Fuels* **1997**, *11* (3), 615−622.
(13) Alboudwarej, H.; Akbarzadeh, K.; Beck, J.; Svrcek, W. Y.; Yarranton, H. W. *AIChE J.* **2003**, *49* (11), 2948−2956.
(14) Wiehe, I. A. *Energy Fuels* **2012**, *26* (7), 4004−4016.
(15) Gonzalez, D. L.; Vargas, F. M.; Mahmoodaghdam, E.; Lim, F.; Joshi, N. *Energy Fuels* **2012**, *26* (10), 6218−6227.
(16) Lin, Y.-J.; He, P.; Tavakkoli, M.; Mathew, N. T.; Fatt, Y. Y.; Chai, J. C.; Goharzadeh, A.; Vargas, F. M.; Biswal, S. L. *Langmuir* **2016**, *32* (34), 8729−8734.
(17) Hosseini-Dastgerdi, Y.; Tabatabaei-Nejad, S. A. R.; Khodapanah, E.; Sahraei, E. *Asia-Pac. J. Chem. Eng.* **2015**, *10* (1), 1−14.
(18) Rao, F.; Liu, Q. *Energy Fuels* **2013**, *27* (12), 7199−7207.
(19) Chaisoontornyotin, W.; Haji-Akbari, N.; Fogler, H. S.; Hoepfner, M. P. *Energy Fuels* **2016**, *30* (3), 1979−1986.
(20) Wang, J.; Buckley, J. S. *Energy Fuels* **2003**, *17* (7), 1445−1451.
(21) Maqbool, T.; Balgoa, A. T.; Fogler, H. S. *Energy Fuels* **2009**, *23* (9), 3681−3686.
(22) Hoepfner, M. P.; Limsakoune, V.; Chuenmeechao, V.; Maqbool, T.; Fogler, H. S. *Energy Fuels* **2013**, *27* (2), 725−735.
(23) Haji-akbari, N.; Masirisuk, P.; Hoepfner, M. P.; Fogler, H. S. *Energy Fuels* **2013**, *27* (5), 2497−2505.
(24) Sandler, S. I. *Chemical, Biochemical, and Engineering Thermodynamics*, 4th ed.; John Wiley & Sons, Inc.: Hoboken, NJ, 2006.
(25) Prasnitz, J. M.; Lichtenthaler, R. N.; Gomes de Azevedo, E. *Molecular Thermodynamics of Fluid-Phase Equilibria*, 3rd ed.; Prentice Hall: Upper Saddle River, NJ, 1999.
(26) Leontaritis, J. Asphaltene Deposition: A Comprehensive Description of Problem Manifestations and Modeling Approaches. *Proceedings of the SPE Production Operations Symposium*; Oklahoma City, OK, March 13−14, 1989; DOI: 10.2118/18892-MS.
(27) Porte, G.; Zhou, H.; Lazzeri, V. *Langmuir* **2003**, *19* (1), 40−47.
(28) Espinat, D.; Ravey, J. C. Colloidal Structure of Asphaltene Solutions and Heavy-Oil Fractions Studied by Small-Angle Neutron and X-Ray Scattering. *Proceedings of the SPE International Symposium on Oilfield Chemistry*; New Orleans, LA, March 2−5, 1993; DOI: 10.2118/25187-MS.
(29) Nabzar, L.; Aguiléra, M. E. *Oil Gas Sci. Technol.* **2008**, *63* (1), 21−35.
(30) Pfeuffer, B.; Kunz, U.; Hoffmann, U.; Turek, T. *Chem. Eng. Technol.* **2009**, *32* (9), 1384−1391.
(31) Storm, D. A.; Baressi, R. J.; Sheu, E. Y. *Energy Fuels* **1995**, *9* (4), 168−176.
(32) Storm, D. A.; Barresi, R. J.; Sheu, E. Y. *Fuel Sci. Technol. Int.* **1996**, *14* (1−2), 243−260.
(33) Sirota, E. B. *Energy Fuels* **2005**, *19* (4), 1290−1296.
(34) Kawanaka, S.; Park, S. J.; Mansoori, G. A. *SPE Reservoir Eng.* **1991**, *6* (02), 185−192.
(35) Sirota, E. B.; Lin, M. Y. *Energy Fuels* **2007**, *21* (5), 2809−2815.
(36) Hirschberg, a.; DeJong, L. N. J.; Schipper, B. a.; Meijer, J. G. *SPEJ, Soc. Pet. Eng. J.* **1984**, *24* (3), 283−293.
(37) Cimino, R.; Correra, S.; Sacomani, P. A.; Carniani, C. Thermodynamic Modelling for Prediction of Asphaltene Deposition in Live Oils. *Proceedings of the SPE International Symposium on Oilfield Chemistry*; San Antonio, TX, Feb 14−17, 1995; pp 499−512, DOI: 10.2118/28993-MS.
(38) Abedini, A.; Ashoori, S.; Torabi, F. *Fluid Phase Equilib.* **2011**, *308* (1−2), 129−134.
(39) Ahmadi, Y.; Kharrat, R.; Hashemi, A.; Bahrami, P.; Mahdavi, S. *Pet. Sci. Technol.* **2014**, *32* (18), 2263−2273.
(40) Abedini, A.; Ashoori, S.; Torabi, F.; Saki, Y.; Dinarvand, N. *J. Pet. Sci. Eng.* **2011**, *78* (2), 316−320.
(41) Hammami, A.; Phelps, C. H.; Monger-McClure, T.; Little, T. M. *Energy Fuels* **2000**, *14* (1), 14−18.
(42) Clarke, P. F.; Pruden, B. B. Heat Transfer Analysis for Detection of Asphaltene Precipitation and Resuspension. *Proceedings of the 47th Annual Technical Meeting of the Petroleum Society*; Calgary, Alberta, Canada, June 10−12, 1996; pp 96−112, DOI: 10.2118/96-112.
(43) Ramos, A. C. S.; Delgado, C. C.; Mohamed, R. S.; Almeida, V. R.; Loh, W. Reversibility and Inhibition of Asphaltene Precipitation in Brazilian Crude Oils. *Proceedings of the 5th Latin American and Caribbean Petroleum Engineering Conference and Exhibition*; Rio de Janeiro, Brazil, Aug 30−Sept 3, 1997; DOI: 10.2118/38967-MS.
(44) Mohammadi, S.; Rashidi, F.; Mousavi-Dehghani, S. A.; Ghazanfari, M. H. *J. Chem. Eng. Data* **2015**, *60* (9), 2646−2654.
(45) Mohamed, R. S.; Loh, W.; Ramos, A. C. S.; Delgado, C. C.; Almeida, V. R. *Pet. Sci. Technol.* **1999**, *17* (7−8), 877−896.
(46) Painter, P.; Veytsman, B.; Youtcheff, J. *Energy Fuels* **2015**, *29*, 2951−2961.
(47) Painter, P.; Veytsman, B.; Youtcheff, J. *Energy Fuels* **2015**, *29* (4), 2120−2133.
(48) Painter, P.; Veytsman, B.; Youtcheff, J. *Energy Fuels* **2015**, *29* (11), 7048−7057.
(49) Caudwell, D. R.; Trusler, J. P. M.; Vesovic, V.; Wakeham, W. a. *J. Chem. Eng. Data* **2009**, *54* (2), 359−366.
(50) Francis, A. *Ind. Eng. Chem.* **1957**, *49* (10), 1779−1786.
(51) Akbarzadeh, K.; Alboudwarej, H.; Svrcek, W. Y.; Yarranton, H. W. *Fluid Phase Equilib.* **2005**, *232* (1−2), 159−170.
(52) Jovanovic, J. D.; Grozdanic, D. K. *J. Serb. Chem. Soc.* **2010**, *75* (7), 997−1003.
(53) Verevkin, S. P.; Tong, B.; Welz-Biermann, U.; Chernyak, Y. *J. Chem. Thermodyn.* **2003**, *35*, 1237−1251.
(54) Nourbakhsh, H.; Yazdizadeh, M.; Esmaeilzadeh, F. *J. Pet. Sci. Eng.* **2011**, *80* (1), 61−68.

DOI: 10.1021/acs.energyfuels.6b02344
Energy Fuels 2017, 31, 3392−3398

CHAPTER 3

COMBINED ASPHALTENE AGGREGATION AND DEPOSITION INVESTIGATION

Reprinted with permission from Chaisoontornyotin, W.; Haji-Akbari, N.; Fogler, H. S.; Hoepfner, M. P. Energy & Fuels 2016, 30 (3), 1979–1986.

energy&fuels

Article

pubs.acs.org/EF

Combined Asphaltene Aggregation and Deposition Investigation

Wattana Chaisoontornyotin,[†] Nasim Haji-Akbari,[‡] H. Scott Fogler,[‡] and Michael P. Hoepfner*[,†]

[†]Department of Chemical Engineering, University of Utah, Salt Lake City, Utah 84112, United States

[‡]Department of Chemical Engineering, University of Michigan, Ann Arbor, Michigan 48109-2136, United States

Supporting Information

ABSTRACT: This study discusses experimental and modeling results of asphaltene aggregation and deposition using various *n*-alkanes as precipitants to destabilize asphaltenes from a crude oil. The amount of asphaltenes precipitated as a function of precipitant carbon number and concentration was obtained after monitoring the slow kinetic aggregation process. A geometric population balance was used to estimate the asphaltene−asphaltene collision efficiency during bulk aggregation. The results revealed that, for a fixed volume fraction of precipitant, the collision efficiency decreases with increasing precipitant carbon number, resulting in slower aggregation. The tendency for asphaltenes to deposit was measured using capillary flow experiments under similar conditions. Similar asphaltene deposition behavior was obtained when the results were normalized by the asphaltene solubility and other experimental factors. A modified aggregation model was applied to the results and revealed that the difference between the asphaltene and solution solubility parameters is a dominant predictor of asphaltene aggregation. The time required to form an initial deposit inside the capillary apparatus was also found to correlate with the difference between asphaltene and solution solubility parameters. However, the deposition rate of asphaltenes in the capillary apparatus did not correlate with the collision efficiency or solubility parameter difference, contrary to initial expectations. The results suggest that mass transport barriers in the apparatus provided sufficient resistance to deposition as to limit observable correlation between the deposition rate and collision efficiency.

INTRODUCTION

Crude oil, or petroleum, is a mixture of hydrocarbons containing a virtually uncountable number of components with different physical and chemical properties.[1] One fraction, asphaltenes, is defined as the portion of crude oil that is soluble in aromatics (e.g., toluene) and insoluble in normal alkanes (e.g., *n*-heptane).[1] Crude oil production rates can be significantly reduced when asphaltenes are destabilized and deposit due to changes in temperature, pressure, and composition.[2−5] A comprehensive understanding of both the asphaltene precipitation and deposition processes is desirable to develop prevention and remediation techniques for asphaltene production problems. Due to the complexity of asphaltene structure and properties,[4,6−13] asphaltene aggregation and deposition have been topics of intense study.

Following the nomenclature used by Hoepfner et al.,[14] a few terms will be defined as follows: (1) "destabilization" is the transition asphaltenes undergo on the nanometer length scale from stable to unstable, or from not able to grow in size to able to grow in size; (2) "aggregation" refers to the transition of the asphaltene size from the nanometer to micrometer length scale; (3) "precipitation" describes the entire process of asphaltenes transitioning from stable nanoaggregates to an unstable material that grows to the micron length scale. Moreover, two additional terms are defined: "aggregation detection time" or "onset time" is the time required for asphaltenes to aggregate to a size of 0.5 μm, detectable by optical microscopy,[15] and "deposition detection time" is the time required until an increase in the pressure drop across a capillary can be detected, indicating an arterial has formed using a capillary deposition apparatus.[14]

Adding precipitants (e.g., *n*-alkanes) to a crude oil is a common technique[14,16,17] to destabilize asphaltenes to validate thermodynamic models[18] and to investigate aggregation and deposition mechanisms. In crude oil production, methane is one compound that can induce asphaltene precipitation. However, it is difficult to study the influence of methane on the asphaltene destabilization processes in the laboratory due to the high pressures required. Instead, liquid *n*-alkanes at ambient conditions are normally used as asphaltene destabilizers.

From previous work, numerous techniques have been used to investigate asphaltene destabilization, such as optical microscopy,[15,19,20] ultraviolet−visible (UV−vis) spectroscopy,[21] small-angle scattering,[16,22] and refractive index measurements.[18,19] Previous studies have shown that slow kinetic aggregation plays an important role in the asphaltene precipitation process.[15,19] These studies revealed that the aggregation detection time using optical microscopy can be weeks or months if the precipitant concentration is sufficiently low.[14,15,17] Additionally, while the instability of asphaltenes at higher precipitant concentrations may be detected over short experimental durations, the final and accurate value of asphaltene solubility may take additional time to measure.[20] Neglecting these kinetic effects will result in inaccurate measurements of the asphaltene stability region and solubility. Moreover, a geometric population balance model has been previously used to model the asphaltene aggregation process and can estimate the particle−particle collision efficiency, β, for asphaltene-asphaltene collisions.[23] The collision efficiency can be described as the number of successful adhesions divided by the total number of collisions, and it has been shown to

Received: October 16, 2015
Revised: January 20, 2016
Published: January 27, 2016

DOI: 10.1021/acs.energyfuels.5b02427
Energy Fuels 2016, 30, 1979−1986

increase exponentially with increasing precipitant concentration.[23] Low collision efficiencies will result in long aggregation detection times and long times for asphaltenes to reach their equilibrium solubility value. This collision efficiency has been related to the aggregation detection time, t_{det}, and the reciprocal of the difference between the asphaltene and surrounding liquid Hildebrand solubility parameters squared, $1/(\delta_{asphaltene} - \delta_{solution})^2$.[17,24−26] These correlations have been developed for asphaltene systems prepared with various asphaltene concentrations,[25] solvents,[17] and precipitants[24] under ambient conditions. These correlations unify the aggregation process for asphaltenes of different origin and at various thermodynamic states into a single framework. The aggregation detection times at ambient temperature (e.g., approximately 20 °C) can be estimated with only knowledge of the solubility parameters of the asphaltenes and the surrounding liquid and the mixture viscosity.[17]

The asphaltene deposition process has been studied with capillary flow measurements,[14,27−31] quartz crystal microbalance,[32,33] a Couette flow apparatus,[34] and other techniques.[5,35−38] It has been previously demonstrated that a capillary deposition apparatus can detect the instability of asphaltenes earlier than a batch process because destabilized asphaltenes are continuously fed into the capillary.[14] Furthermore, the capillary deposition apparatus has been shown to detect deposition at asphaltene contents as low as 0.04 wt %,[27] demonstrating the sensitivity of the technique. With the capillary apparatus, oil and a precipitant are mixed and flown through a capillary tube, generally glass or metallic. The formation of asphaltene deposits inside the tube wall restricts the flow that can be detected by an increase in the pressure drop across the capillary (i.e., differential pressure). If the deposit is assumed to be axially uniform, the pressure drop measurement can be related to a deposit thickness. However, there are conflicting results as to whether assuming a uniform deposit along the tube length is appropriate, as it is likely dependent on the apparatus design.[28,31,39] The apparatus used in the present investigation has been previously shown to produce nonuniform deposits due to the deposition process occurring in the mass transfer entrance region.[14] In the mass transfer entrance region, the concentration gradient of destabilized asphaltenes at the wall, which governs the deposition rate, will vary significantly with axial position.[40] Due to the nonuniform deposit profile of the apparatus used for this investigation, the presented results herein were not converted to a deposit thickness, but rather the scaled pressure drop will serve as a representation of the deposition rate. The influence of the precipitant carbon number on asphaltene deposition was previously investigated using three different *n*-alkanes and as a function of precipitant concentration.[28,29] It was found that the deposition rate increases with decreasing precipitant carbon number, and that the deposition rate is affected by the precipitant concentration. These results did not consider the influence of the carbon number on asphaltene solubility, where at high precipitant concentrations, asphaltene precipitation increases with decreasing precipitant carbon number.[41] Previous work has shown that an increased quantity of destabilized asphaltenes (i.e., low solubility) will result in an increased deposition rate.[14] Isolation of the effect of the precipitant carbon number from its influence on asphaltene solubility could provide new insight into the asphaltene deposition process.

The overarching objective of this investigation is to study the aggregation, precipitation and deposition of asphaltenes as a function of the *n*-alkane precipitant carbon number and concentration. Another purpose is to investigate relationships between kinetic aggregation, deposition, and the solubility parameter. This approach is comprehensive and investigates both the asphaltene aggregation and deposition processes rather than studying them independently. A previously developed correlation was used to estimate the asphaltene solubility parameter from aggregation detection time measurements.[17,24,25] However, in this study, the measured mass of asphaltenes precipitated vs time were analyzed with a geometric population balance model[23] to estimate the asphaltene-asphaltene collision efficiency. The deposition behavior of asphaltenes was assessed by monitoring the pressure drop across a capillary deposition apparatus. The number of techniques applied in this study, coupled with the variations in precipitant carbon number and concentration, resulted in a robust and comprehensive study of asphaltene behavior.

■ EXPERIMENTAL METHODS

Prior to experimentation, the crude oil used in this investigation, Oil A, was centrifuged at 10,000 rpm for 3 h to separate solid contaminant particles and water. Oil A was collected at the wellhead and contained no production additives that are used to prevent deposition or corrosion. All liquid diluents (e.g., toluene and *n*-alkanes) were high performance liquid chromatography (HPLC)-grade and supplied from Fisher Scientific. All precipitants used were *n*-alkanes and for brevity may be referred to by their respective carbon number (e.g., C7 for *n*-heptane).

Asphaltene Aggregation and Solubility. Following the procedure of Maqbool et al.,[20] a precipitant was slowly added to a continuously stirred volume of crude oil by a Harvard apparatus 22 Syringe pump until the desired precipitant concentration was obtained. Samples were prepared at ambient temperature and then placed in a water bath that was controlled at a temperature of 60 °C for the duration of the experiment.[20] Samples were continuously stirred using Teflon coated magnetic stir bars to prevent particle setting. Evaporation losses were minimized by storing samples in vials with mininert push-button valves that were punctured with a needle to draw samples. At various times (t_1, t_2, t_3, etc.) samples were taken from the diluted crude oil and transferred to two 1.5 mL microcentrifuge tubes. The microcentrifuge tubes were centrifuged using an Eppendorf 5418 Micro Centrifuge at 14,000 rpm (16,000 g-force) for 10 min to separate the precipitated asphaltenes. The supernatant was removed and additional precipitant was added to the asphaltene cake in order to remove any entrained crude oil. The solid asphaltene cake was sonicated using a Branson 1510 Sonicator for approximately 10−20 min with the fresh precipitant in order to disrupt the solid cake and aid in the washing process. The asphaltene cake was washed repeatedly with fresh precipitant until the supernatant was colorless. The cake was then dried in an oven at 75 °C until the mass was constant and the weight of precipitated asphaltenes was measured. In order to carefully consider the kinetic aggregation effect, this procedure was repeated until the mass of asphaltenes separated from the diluted crude oil was constant as a function of mixing time with a precipitant.

A previously published geometric population balance model[23] was used to estimate the asphaltene-asphaltene collision efficiency, β, from the mass precipitated vs time results, described above. The model simulates the growth of asphaltene aggregates from the nanometer to micrometer size and detail can be found elsewhere.[23] The only unknown parameter in the model is the collision efficiency, which is calculated using the best fit between the simulation and experimental results. The best fit for β is the value that minimized the Sum Square Error (SSE) between the predicted and measured results, which is the summation of the squared difference between the experimental data and the estimated results from the model. Lower values of SSE suggest a better theoretical fit to the data. To obtain an estimate of the uncertainty in the collision efficiency, the mass precipitated vs time results were divided into 2 sections: the first 35% of the data points as

DOI: 10.1021/acs.energyfuels.5b02427
Energy Fuels 2016, 30, 1979−1986

a function of time comprises the first section and the remainder of the data is the second section. The asphaltene precipitation rate is rapid at short mixing times, and the first 35% of the data points were selected to characterize this behavior. The collision efficiency obtained using the complete data set was selected as the primary measurement, and the results from the two divided sections, beginning and end, were used as the upper and lower bounds of the uncertainty estimate. An example of a model fit using the multiple sections and the parameter values used in the population balance model can be found in the Supporting Information.

Asphaltene Solubility Parameter. To obtain the asphaltene solubility parameter, the aggregation detection time was measured and the surrounding liquid's solubility parameter was estimated. To measure the aggregation detection time, a precipitant was slowly added to a continuously stirred volume of crude oil until the desired precipitant concentration was obtained. The samples were prepared at ambient temperature and then placed in a water bath that was controlled at a temperature of 60 °C. This initial procedure mimics that described above for the aggregation samples; however, instead of centrifuging the samples, they were observed under a Nikon Eclipse E600 optical microscope. The time it took for asphaltenes to reach a size of 0.5 μm was recorded as the aggregation detection time.

The solubility parameters of Oil A and *n*-alkanes at 60 °C were estimated using their refractive indices on a Schmidt and Haensch DUR-HT refractometer. The correlation developed by Wang et al.[18] was used to relate the refractive index of the solution to its Hildebrand solubility parameter. A volumetric average of the solubility parameters of the components was used to determine the solution solubility parameter ($\delta_{solution}$). The asphaltene solubility parameter ($\delta_{asphaltene}$) was estimated using a modified version of the correlation between the aggregation detection time and $1/(\delta_{asphaltene}-\delta_{solution})^2$ established by Haji-Akbari et al.[17] The correlation developed by Haji-Akbari et al.[17] was for experiments performed at ambient temperature, assumed constant at 20 °C, and modifications were required to apply it for systems at 60 °C, the temperature used in this study. More detail on the modification procedure is found in the Supporting Information. Furthermore, the asphaltene solubility parameter was varied for each *n*-alkane precipitant, as has been done previously,[24] using the modified correlation at 60 °C as a method to approximate the different properties of asphaltenes precipitated using various *n*-alkanes.

Asphaltene Deposition. A capillary deposition apparatus, previously reported by Hoepfner et al.,[14] was used to assess the deposition tendencies of asphaltenes as a function of precipitant carbon number and concentration. The apparatus operates by forcing a mixture of oil and precipitant through a metallic capillary while monitoring the differential pressure. The procedure to operate the apparatus was unmodified from the previous study, and readers are referred to ref 14. for full detail. The flow rates of precipitant and Oil A were controlled using two separate Teledyne ISCO Model 500D Syringe pumps, and the total flow rate for all experiments was held constant at 5 mL/h regardless of the composition. All experiments were in the laminar flow regime with Reynolds numbers varying between 2 and 3 depending on the mixture viscosity. The individual flow rates were adjusted to achieve the desired precipitant concentration and the capillary and mixing system were operated in a Cole-Parmer Polystat Heated Circulating Bath maintained at 60 °C. The pressure drop across the capillary was measured as a function of time using Sensotec A-5/882−15 pressure transducer. A FEL Quanta 200 3D Scanning Electron Microscopy (SEM) operating at 0.45 Torr in low vacuum mode was used to visualize the capillary inlet to assess the deposit's radial uniformity and thickness at the capillary entrance. The deposit's radial uniformity was used to assess the quality of mixing between oil and precipitant. Highly asymmetric deposits were interpreted as being generated by nonhomogenized solutions because incomplete mixing would result in regions with higher than anticipated concentrations of *n*-alkane precipitant, and consequently, thicker deposits.

Clean and unused capillaries with a nominal inner diameter (ID) of 0.01 in. and length of 5 cm were used for each new experiment. Prior to performing a deposition experiment, the ID of each unmodified capillary (Upchurch Scientific, part: U-101) was determined by measuring the pressure drop across the capillary when flowing deionized water through the system at 25 °C at flow rates of 0.5, 1, 3, and 5 mL/min. The Hagan-Poiseuille equation was linearized by plotting the flow rate vs pressure drop, and a linear regression was used to determine the capillary ID. Capillaries were dried after measuring their inner diameter with water and were only used once (i.e., a new capillary was characterized and used for each deposition experiment). The deposition detection time, t_D, was estimated as the point where an increase in the pressure drop was observed to be larger than the statistical variation in the transducer measurement.

■ RESULTS AND DISCUSSION

Asphaltene Aggregation. The percentage of Oil A that precipitated (i.e., asphaltenes) after mixing with an *n*-alkane precipitant as a function of time at 60 °C is shown in Figure 1.

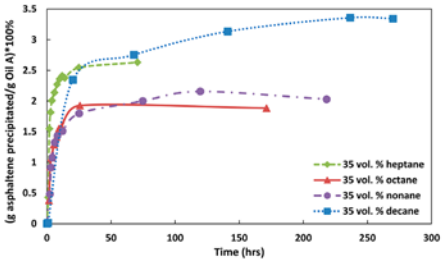

Figure 1. Mass percentage of precipitated asphaltene from Oil A at 60 °C for 35 vol % heptane, octane, nonane, and decane. Error bars are smaller than the markers. Dashed lines are to guide the eyes.

Additional results are presented in the Supporting Information. It was found that the times required for the amount of precipitated asphaltenes to reach their equilibrium value were approximately 70, 170, 200, and 270 h for 35 vol % of C7, C8, C9 and C10, respectively. This result suggests that the time required for the solubility of asphaltenes to be measured accurately increases for higher precipitant carbon numbers. One possible explanation for this observation is that the viscosity increases with carbon number, which would result in slower asphaltene diffusion, fewer asphaltene-asphaltene collisions, and ultimately longer aggregation detection times. An alternative analysis approach is to use the collision efficiency as measured with the geometric population balance model, and the results will be discussed momentarily. The collision efficiency accounts for the reduced diffusivity in higher viscosity systems and represents a direct indicator of the role of precipitant carbon number on the interaction between two asphaltenes.

The equilibrium values for the mass of precipitated asphaltenes from Oil A as a function of precipitant carbon number are plotted in Figure 2 for a constant precipitant concentration of 35 vol %. Due to the low volatility of decane, it is possible that some amount of decane might have been trapped inside precipitated asphaltenes, resulting in an artificially raised precipitated mass. However, the measured mass of precipitated asphaltenes remained constant at the end of the drying process, suggestive that all decane had been removed. The results from Figure 2 reveal that the solubility of asphaltenes in various *n*-alkane precipitants was approximately constant at low precipitant concentrations. *This finding is in*

DOI: 10.1021/acs.energyfuels.5b02427
Energy Fuels 2016, 30, 1979−1986

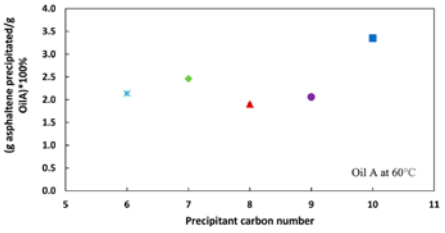

Figure 2. Equilibrium value for the mass of precipitated asphaltenes from Oil A for 35 vol % hexane, heptane, octane, nonane, and decane as a function of precipitant carbon number.

contrast to the established trend of decreasing solubility with decreasing precipitant carbon number at high precipitant concentrations.[1,41] Similar behavior has been identified with a different crude oil in a previous investigation.[42] The previous study[42] also demonstrated that as the precipitant concentration is increased above 70 vol %, the traditional trend of decreasing solubility (i.e., increased mass precipitated) as the carbon number is decreased is re-established.[1,41] The factors that make the quantity of asphaltenes precipitating independent of the precipitant carbon number at low precipitant concentrations have not been fully explored; however, the authors believe that future investigation of this phenomenon could produce improved theoretical understanding of the asphaltene destabilization process.

The solubility parameters of Oil A and the pure components used in this investigation were obtained as described previously using refractive index measurements, and the results are shown in Table 1. The results for the pure species were within 1.5% of

Table 1. Solution Solubility Parameter at 60 °C for Various Precipitants and Volume % Precipitants in Oil A

Component	Hildebrand solubility parameter ($MPa^{0.5}$)	Precipitant concentration (in vol %)	Mixture solubility parameter ($MPa^{0.5}$)
Oil A	18.3		
Heptane	14.6	30	17.2
		35	17.0
Octane	14.9	35	17.1
Nonane	15.1	35	17.2
Decane	15.3	35	17.3
		40	17.1

their literature values.[43] The asphaltene solubility parameters were estimated using aggregation detection time measurements and the correlation developed by Haji-Akbari et al.[17] The aggregation detection time for Oil A at 60 °C with 35 vol % C7, C8, C9, and C10 are 140 ± 36, 250 ± 30, 280 ± 4, and 380 ± 20 min, respectively. These results were fit to the modified Haji-Akbari correlation and the resulting asphaltene solubility parameter measurements as a function of precipitant carbon number are shown in Figure 3. It can be observed that the asphaltene solubility parameter increases with increasing precipitant carbon number, in agreement with previous work.[24] This trend is believed to be due to the polydispersity of asphaltenes and is discussed in detail by Haji-Akabri et al.[24] Although the solubility of asphaltenes was measured to be approximately constant as a function of the precipitant carbon

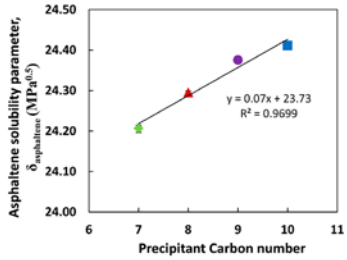

Figure 3. Asphaltene solubility parameters as a function of the precipitant carbon number for asphaltenes precipitated from Oil A at 60 °C.

number, the asphaltene solubility parameter was still allowed to vary with precipitant type. While different precipitants may destabilize a similar quantity of asphaltenes, it is not apparent whether these asphaltenes have identical properties or if they each consist of different subfractions. Varying the asphaltene solubility parameters as a function of precipitant carbon number approximates this collective behavior. Future investigation is prudent to further explore the observed trend of the solubility parameter as a function of the precipitant carbon number and potential limitations of this approach. In order to obtain the asphaltene solubility parameter for hexane, C6, the linear correlation between the asphaltene solubility parameter and precipitant carbon number presented in Figure 3 was extrapolated to C6. It was estimated that the asphaltene solubility parameter for hexane is 24.2 $MPa^{0.5}$ at 60 °C.

The mass precipitated vs time results, Figure 1, and the geometric population balance model were used to estimate the asphaltene−asphaltene collision efficiency during precipitation. Figure 4 shows the best fits and uncertainty of the collision

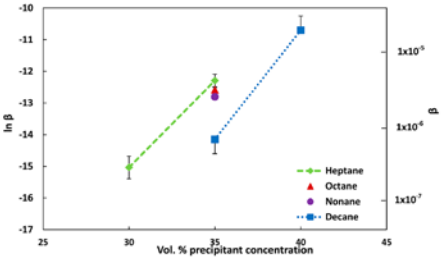

Figure 4. Collision efficiency at minimum SSE as determined by the geometric population balance with min-max error bars for Oil A at 60 °C as a function of precipitant and precipitant concentration.

efficiency for Oil A at 60 °C as a function of the precipitant carbon number and concentration. For a fixed volume fraction of precipitant, the collision efficiency decreases by approximately 25%, 40%, and 84% when the precipitant carbon number increases from C7 to C8, C9, and C10 respectively. In addition, decreasing the precipitant concentration resulted in a lower collision efficiency, which is consistent with previous work.[23] These findings can be readily explained by considering

DOI: 10.1021/acs.energyfuels.5b02427
Energy Fuels 2016, 30, 1979−1986

that the Hildebrand solubility parameter increases with increasing carbon number.[24,44] At a fixed volume fraction of precipitant, the Hildebrand solubility parameter of the oil-precipitant mixture increases with increasing carbon number, reducing the difference between the mixture and the asphaltene solubility parameters (Table 1). The smaller difference between the asphaltene and mixture solubility parameter results in a weaker driving force for precipitation and lower collision efficiency as the carbon number is increased. At a fixed precipitant carbon number, the Hildebrand solubility parameter of the oil-precipitant mixture decreases with increasing precipitant concentration. This effect increases the difference between asphaltene and mixture solubility parameter, which creates a larger driving force for precipitation, and results in a higher collision efficiency value.

The collision efficiencies shown in Figure 4 were replotted against $1/(\delta_{asphaltene}-\delta_{solution})^2$ for Oil A at 60 °C using the asphaltene solubility parameter measured with the modified aggregation detection time correlation. This plot, shown in Figure 5, demonstrates the excellent correlation that is obtained

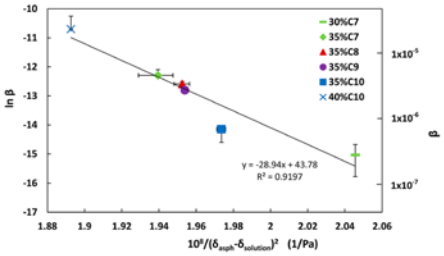

Figure 5. Correlation between collision efficiency and $1/(\delta_{asphaltene} - \delta_{solution})^2$ for Oil A at 60 °C.

between the collision efficiencies at the different solution solubility parameters without any additional modification of the measured parameters. *This result reveals that differences in the kinetic aggregation process, as interpreted by the collision efficiency measured using a population balance model, can be collapsed to a single unifying line regardless of the precipitant or precipitant concentration used.* This correlation reinforces the similar asphaltene aggregation behavior established previously,[17,24,25] which used the aggregation detection time as the basis for estimating asphaltene-asphaltene collision efficiency. The similar trends observed in the collision efficiency as inferred through the aggregation detection time and using a geometric population balance model emphasize the robustness of this approach. In addition, these findings provide a new tool to predict the collision efficiency of other asphaltene systems without committing to long duration experiments with slow kinetics.

Asphaltene Deposition. Asphaltene deposition was induced by the addition of C6, C7, C8, and C10 precipitants to Oil A inside the capillary deposition apparatus. All mixtures produced consistent and reproducible pressure drop trajectories, save for the experiments performed with C10. The pressure drop vs time results for Oil A diluted with C10 were inconsistent as observed by poor reproducibility and large fluctuations in the pressure drop (examples are shown in the Supporting Information). Incomplete mixing between Oil A and C10 was suspected to be the primary cause of these inconsistent results. Decane has a higher viscosity and consequently lower diffusivity when compared to the other precipitants used,[45] and is expected to require longer contact times inside the apparatus to fully mix. Images taken by SEM of the deposit at the capillary inlet for experiments with 35 vol % C10 in Oil A are shown in Figure 6. These images reveal an asymmetric radial deposit, demonstrating incomplete mixing of oil and precipitant. The bridge-shaped deposit (image 6b) is likely caused by the stratified flow of partially mixed oil-rich and decane-rich fluids, where the deposit bridge is formed at the junction of these two fluids. Moreover, SEM images of the deposit at the capillary inlet using C6, C7, and C8 as precipitants revealed a deposit had formed around the entire capillary inlet, within reproducibility, suggestive of proper mixing. An example of good mixing using C8 as the precipitant is shown in Figure 6d, which is in agreement with previous work that utilized C7 to destabilize asphaltenes.[14]

The pressure drop through the capillary deposition apparatus was normalized by mixture viscosity (μ), mass fraction of insoluble asphaltenes (F, grams of insoluble asphaltenes per gram of crude oil), and crude oil volume fraction ($\varnothing_{oil}$) for each precipitant and precipitant concentration. This normalization procedure follows the approach reported previously[14] with the modification to also include normalization by the initial capillary radius to the forth power (r^4). The Hagen-Poiseille equation reveals that the pressure drop through a circular duct is inversely proportional to the radius to the fourth power and proportional to the viscosity. The normalization by the initial capillary radius corrected for differences in capillary geometry between experimental runs. However, normalization by viscosity might be varied if the deposit is highly nonuniform and forms an orifice-like profile because the pressure drop might not be proportional to the viscosity.[46] Figure 7 shows the normalized pressure drop trajectories for Oil A at 60 °C as a function of precipitant and precipitant concentration. It is to be noted that a direct comparison between the normalized pressure drop results in this investigation and previous work[14] is shown in the Supporting Information, demonstrating

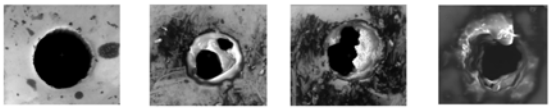

Figure 6. SEM images of the deposit at the capillary inlet for: (a) an unused capillary, (b) a deposit generated with 35 vol % C10 in Oil A (poor mixing), (c) an additional deposit generated with 35 vol % C10 in Oil A (poor mixing), (d) a deposit generated with 35 vol % C8 in Oil A (fully mixed).

DOI: 10.1021/acs.energyfuels.5b02427
Energy Fuels 2016, 30, 1979−1986

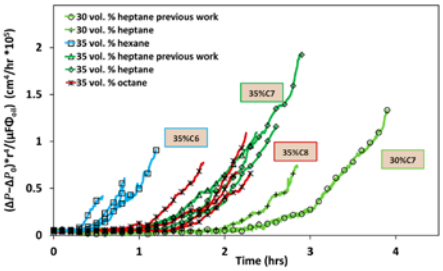

Figure 7. Normalized pressure drop trajectories for Oil A at 60 °C diluted with various precipitants and precipitant concentrations. (Previous results from Hoepfner et al.[14])

reliable and consistent results. It can be observed in Figure 7 that the deposition detection time is 1.9 ± 0.2 h at 30 vol % C7 and 0.94 ± 0.08 h at 35 vol % C7, revealing that *at a fixed precipitant carbon number, high precipitant concentrations result in a faster deposition detection time.* Moreover, it can be seen that the deposition detection time increases from 0.25 ± 0.05 h for C6 to 0.94 ± 0.08 h for C7 and to 1.05 ± 0.31 h for C8 at 35 vol % of precipitant. *This finding reveals that at a constant precipitant concentration, higher carbon number precipitants have weaker destabilizing effects on asphaltenes, which leads to longer deposition detection times.* This trend can be explained using the same analysis approach as was performed with the collision efficiency, where lower carbon number precipitants at a fixed volume fraction produce a mixture with an overall lower the Hildebrand solubility parameter. The propensity for asphaltenes to adsorb on the surface of the metal is characterized in the deposition detection time, with a high propensity for adsorption producing a short deposition detection time. Consequently, the driving force for asphaltenes to adsorb on metallic surfaces increases as the difference in asphaltene and mixture solubility parameter increases, and follows a similar trend as bulk asphaltene aggregation.

In order to generalize the deposition results, the deposition detection time was plotted against $1/(\delta_{asphaltene}\text{-}\delta_{solution})^2$ and the result is shown in Figure 8. It was found that $1/(\delta_{asphaltene} - \delta_{solution})^2$ and the deposition detection time are highly correlated, demonstrating that the difference between asphaltene and mixture solubility parameters plays a dominant role in

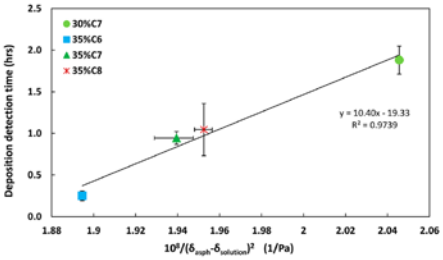

Figure 8. Correlation between deposition detection time and $1/(\delta_{asphaltene} - \delta_{solution})^2$ for Oil A at 60 °C.

the rate of asphaltene adsorption. This finding suggests that by knowing the difference between the asphaltene and surrounding liquid solubility parameters, asphaltene deposition detection time can be predicted and estimated, reducing future experimental burden. Furthermore, this result can be used to predict the asphaltene solubility parameter through the course of a capillary deposition experiment.

The pressure drop profiles in Figure 7 were averaged based on their precipitant carbon number and concentration and shifted by their deposition detection time. The result of this procedure is shown in Figure 9 and demonstrates similar

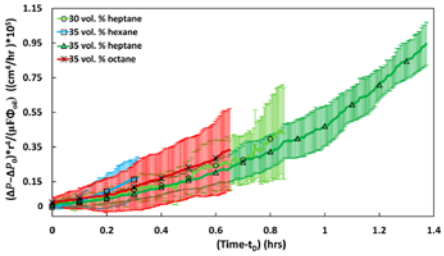

Figure 9. Averaged and normalized pressure drop trajectories for Oil A at 60 °C for various precipitants and precipitant concentrations after eliminating the deposition detection time, t_D. Error bars represent the minimum and maximum values before averaging.

behavior, within experimental reproducibility, regardless of the precipitant type or concentration used. The error bars indicate the minimum and maximum values of the pressure drop trajectories before the averaging process. The slopes of all pressure drop trajectories are approximately the same after the pressure drop was normalized using r^4, μ, F, and Φ_{oil} and when the deposition detection time, t_D, is eliminated from the results.

The results in Figure 9 stand in contrast to the findings presented above for the deposition detection time (Figure 8) and collision efficiency (Figure 5), where the rate of adsorption and aggregation were dependent on the mixture solubility parameter. The deposition rate was not observed to depend on the mixture environment, beyond its influence on the solubility of asphaltenes. The normalized deposition profiles differ by less than a factor of 2 while the collision efficiencies vary by nearly a factor of 10. From this observation, it is clear that inclusion of the collision efficiency differences between samples would disrupt the observed uniform deposition behavior. This finding was in contrast to initial expectations that deposition rate should be a function of $1/(\delta_{asphaltene}\text{-}\delta_{solution})^2$ or the collision efficiency. This result suggests that asphaltene-deposit interactions are not the rate-controlling step for the deposition process inside the capillary apparatus. If the limiting step to deposition were the asphaltene-deposit collision efficiency (i.e., the probability of a destabilized aggregate adhering to the deposit during a collision), the deposition rate would be expected to scale with the bulk aggregation collision efficiency. However, because this phenomenon was not observed, diffusion rates, shear inhibition[30,34] or other barriers to deposition limit the deposition rate inside the capillary apparatus. This finding highlights the complex influence that device geometry plays into assessing the rate controlling step in the asphaltene deposition processes. However, in bulk

DOI: 10.1021/acs.energyfuels.5b02427
Energy Fuels 2016, 30, 1979−1986

aggregation, the diffusion time between asphaltene aggregates is short and collisions frequent enough that the collision efficiency correlates well with $1/(\delta_{asphaltene}-\delta_{solution})^2$. In summary, the rate of initial deposit formation (i.e., induction or deposition detection time) is related to the difference between the asphaltene and solution solubility parameters, but the rate of deposit growth (i.e., multilayer formation) is hindered by diffusion limitations or other barriers.

CONCLUSION

Asphaltene aggregation and deposition were studied using various precipitants and precipitant concentrations, and the following conclusions were found:

(1) The solubility of asphaltenes in various *n*-alkane precipitants is approximately constant at low precipitant concentrations when the slow kinetic effects on the solubility measurements are considered by measuring at the equilibrium state.

(2) For a fixed precipitant volume fraction, the asphaltene–asphaltene collision efficiency decreases with increasing precipitant carbon number. Decreasing the precipitant concentration results in lower collision efficiency.

(3) The collision efficiency measurements are highly correlated with $1/(\delta_{asphaltene} - \delta_{solution})^2$ for Oil A at 60 °C.

(4) Similar asphaltene deposition behavior is obtained under drastically different conditions after correcting for differences in asphaltene solubility, mixture viscosity, and capillary geometry.

(5) Shorter deposition detection times are observed using precipitants with lower carbon numbers, and at higher precipitant concentrations. The deposition detection time also correlates with $1/(\delta_{asphaltene} - \delta_{solution})^2$.

(6) The differences in collision efficiency for bulk aggregation with different precipitants and precipitant concentrations did not appear to influence the normalized deposition behavior. This finding suggests that transport limitations or other barriers influence the rate of asphaltene deposition even in a narrow capillaries.

ASSOCIATED CONTENT

Supporting Information

The Supporting Information is available free of charge on the ACS Publications website at DOI: 10.1021/acs.energyfuels.5b02427.

Mass percentage of asphaltenes precipitated from Oil A at 60 °C when diluted to 30 vol % heptane and 40 vol % decane, values of parameters used in the population balance model, collision efficiency uncertainty, and normalized pressure drop trajectory. (PDF)

AUTHOR INFORMATION

Corresponding Author

*E-mail: michael.hoepfner@utah.edu.

Notes

The authors declare no competing financial interest.

ACKNOWLEDGMENTS

The authors would like to thank Thanawat Thanthong, Thammaporn Somkhan, and Cláudio Vilas Bôas FáVero for helpful discussion and suggestions. In addition, this work was funded in part by the University of Michigan Industrial Affiliates Program, whose members include Chevron, ConocoPhillips, MSi Kenny, NALCO, BP, Shell, Statoil, and Total.

REFERENCES

(1) Speight, J. *The chemistry and technology of petroleum*, 4 th ed.; Taylor and Francis Group, LLC: Florida, 2007.
(2) Gonzalez, D. L.; Ting, P. D.; Hirasaki, G. J.; Chapman, W. G. *Energy Fuels* **2005**, *19* (4), 1230–1234.
(3) Vargas, F. M.; Gonzalez, D. L.; Hirasaki, G. J.; Chapman, W. G. *Energy Fuels* **2009**, 23 (6), 1140–1146.
(4) Creek, J. *Energy Fuels* **2005**, *19* (4), 1212–1224.
(5) Hammami, A.; Ratulowski, J. *Asphaltenes, Heavy Oils, and Petroleomics* **2007**, 617–660.
(6) Sirota, E. B. *Energy Fuels* **2005**, *19* (4), 1290–1296.
(7) Mullins, O. C.; Sabbah, H.; Pomerantz, A. E.; Barre, L.; Andrews, a B.; Ruiz-morales, Y.; Mostowfi, F.; Mcfarlane, R.; Goual, L.; Lepkowicz, R.; Cooper, T.; Orbulescu, J.; Leblanc, R. M.; Edwards, J.; Zare, R. N. *Energy Fuels* **2012**, *26*, 3986–4003.
(8) Mullins, O. C.; Seifert, D. J.; Zuo, J. Y.; Zeybek, M. *Energy Fuels* **2013**, *27* (4), 1752–1761.
(9) Oh, K.; Deo, M. D. *Asphaltenes, Heavy Oils, and Petroleomics* **2007**, 469–488.
(10) Tanaka, R.; Sato, E.; Hunt, J. E.; Winans, R. E. *Energy Fuels* **2004**, *18* (4), 1118–1125.
(11) Yen, T. F.; Erdman, J. G.; Pollack, S. S. *Anal. Chem.* **1961**, 33 (11), 1587–1594.
(12) Andersen, S. I.; Jensen, J. O.; Speight, J. G. *Energy Fuels* **2005**, *19* (6), 2371–2377.
(13) Eyssautier, J.; Levitz, P.; Espinat, D.; Jestin, J.; Gummel, J.; Grillo, I.; Barré, L. J. *J. Phys. Chem. B* **2011**, *115* (21), 6827–6837.
(14) Hoepfner, M. P.; Limsakoune, V.; Chuenmeechao, V.; Maqbool, T.; Fogler, H. S. *Energy Fuels* **2013**, *27* (2), 725–735.
(15) Maqbool, T.; Balgoa, A. T.; Fogler, H. S. *Energy Fuels* **2009**, 23 (9), 3681–3686.
(16) Sirota, E. B.; Lin, M. Y. *Energy Fuels* **2007**, *21* (5), 2809–2815.
(17) Haji-akbari, N.; Masirisuk, P.; Hoepfner, M. P.; Fogler, H. S. *Energy Fuels* **2013**, *27* (5), 2497–2505.
(18) Wang, J. X.; Buckley, J. S. *Energy Fuels* **2001**, *15* (5), 1004–1012.
(19) Wang, J.; Buckley, J. S. *Energy Fuels* **2003**, *17* (7), 1445–1451.
(20) Maqbool, T.; Srikiratiwong, P.; Fogler, H. S. *Energy Fuels* **2011**, *25* (2), 694–700.
(21) Kraiwattanawong, K.; Fogler, H. S.; Gharfeh, S. G.; Singh, P.; Thomason, W. H.; Chavadej, S. *Energy Fuels* **2007**, *21* (3), 1248–1255.
(22) Hoepfner, M. P.; FáVero, C. V. B.; Haji-Akbari, N.; Fogler, H. S. *Langmuir* **2013**, *29* (28), 8799–8808.
(23) Maqbool, T.; Raha, S.; Hoepfner, M. P.; Fogler, H. S. *Energy Fuels* **2011**, *25* (4), 1585–1596.
(24) Haji-Akbari, N.; Teeraphapkul, P.; Balgoa, A. T.; Fogler, H. S. *Energy Fuels* **2015**, *29*, 2190.
(25) Haji-Akbari, N.; Teeraphapkul, P.; Fogler, H. S. *Energy Fuels* **2014**, *28* (2), 909–919.
(26) Haji-Akbari, N. *Destabilization and Aggregation Kinetics of Asphaltenes*; University of Michigan: 2014.
(27) Broseta, D.; Robin, M.; Savvidis, T.; Féjean, C.; Français, L.; Durandeau, M.; Zhou, H. Detection of Asphaltene Deposition by Capillary Flow Measurements. In *SPE/DOE Improved Oil Recovery Symposium*, 3-5 April, Tulsa, Oklahoma; Society of Petroleum Engineers: 2000; DOI: 10.2118/59294-MS.
(28) Wang, J.; Buckley, J. S.; Creek, J. L. *J. Dispersion Sci. Technol.* **2004**, *25* (3), 287–298.
(29) Lawal, K. a.; Crawshaw, J. P.; Boek, E. S.; Vesovic, V. *Energy Fuels* **2012**, *26* (4), 2145–2153.
(30) Nabzar, L.; Aguiléra, M. E. *Oil Gas Sci. Technol.* **2008**, *63* (1), 21–35.
(31) Boek, E. S.; Ladva, H. K.; Crawshaw, J. P.; Padding, J. T. *AIP Conf. Proc.* **2008**, *1027* (4), 273–275.
(32) Tavakkoli, M.; Panuganti, S. R.; Vargas, F. M.; Taghikhani, V.; Pishvaie, M. R.; Chapman, W. G. *Energy Fuels* **2014**, *28* (3), 1617–1628.

DOI: 10.1021/acs.energyfuels.5b02427
Energy Fuels 2016, 30, 1979–1986

(33) Tavakkoli, M.; Panuganti, S. R.; Taghikhani, V.; Pishvaie, M. R.; Chapman, W. G. *Energy Fuels* **2014**, *28* (6), 3594−3603.
(34) Eskin, D.; Ratulowski, J.; Akbarzadeh, K.; Pan, S. *Can. J. Chem. Eng.* **2011**, *89* (June), 421−441.
(35) Zougari, M.; Jacobs, S.; Ratulowski, J.; Hammami, A.; Broze, G.; Flannery, M.; Stankiewicz, A.; Karan, K. *Energy Fuels* **2006**, *20* (4), 1656−1663.
(36) Alboudwarej, H.; Svrcek, W. Y.; Kantzas, A.; Yarranton, H. W. *Pet. Sci. Technol.* **2004**, *22* (7−8), 799−820.
(37) Hu, C.; Morris, J. E.; Hartman, R. L. *Lab Chip* **2014**, *14* (12), 2014−2022.
(38) Hu, C.; Hartman, R. L. *AIChE J.* **2014**, *60*, 3534−3546.
(39) Boek, E. S.; Wilson, A. D.; Padding, J. T.; Headen, T. F.; Crawshaw, J. P. *Energy Fuels* **2010**, *24* (4), 2361−2368.
(40) Deen, W. M. *Analysis of Transport Phenomena* **1998**.
(41) Mitchell, D. L.; Speight, J. G. *Energy Fuels* **1972**, *52* (2), 149−152.
(42) Srikiratiwong, P. *Effects of n-Alkane Precipitants and Temperature on the Kinetics of Asphaltene Precipitation*; The Petroleum and Petrochemical College, Chulalongkorn University: 2010.
(43) Akbarzadeh, K.; Alboudwarej, H.; Svrcek, W. Y.; Yarranton, H. W. *Fluid Phase Equilib.* **2005**, *232* (1−2), 159−170.
(44) Barton, A. F. M. *Handbook of Solubility Parameters and Other Cohesion Parameters* **1991**.
(45) Hayduk, W.; Minhas, B. S. *Can. J. Chem. Eng.* **1982**, *60* (2), 295−299.
(46) Nevers, N. de. *Fluid Mechanics for Chemical Engineers*, 3rd ed.; McGraw-Hill, 2005.

DOI: 10.1021/acs.energyfuels.5b02427
Energy Fuels 2016, 30, 1979−1986

CHAPTER 4

KINETIC PRECIPITATION OF ASPHALTENES WITH THE PRESENCE OF INORGANIC SOLIDS IN BITUMEN

4.1 Introduction

Asphaltenes are the heaviest and most polar fraction of crude oil and are defined as the material that is soluble in aromatic solvents (toluene) and insoluble in n-alkanes (n-heptane).[1–4] Asphaltenes generally consist of a polyaromatic core with various alkyl side chains and contain heteroatoms (N, S, and O) and trace metals (e.g., Ni, V, and Fe).[5] Changes in pressure, temperature, and composition during oil or bitumen production and processing can destabilize asphaltenes.[3,4,6–9] Destabilized asphaltenes can precipitate and deposit in processing and refining equipment leading to decreases in oil productivity, production downtime, and downstream issues such as fouling in heat exchangers.[5,7,8,10,11]

In the bitumen hot water extraction process, bitumen froth is formed with an approximate composition of 60 wt% bitumen, 30 wt% water, and 10 wt% inorganic solids.[11–17] In this work, the term “inorganic solids” or “solids” will refer to the non-asphaltenic solids, including clay mineral, and other insoluble organic matter. In Athabasca bitumen, the dominant component of clay minerals is 69 wt% kaolinite and 28 wt% illite with specific surface area, SSA, of 10-20 and 65-100 m^2/g, respectively.[12] A diluent (e.g., naphtha or n-paraffin) is added to the froth to reduce the viscosity of the oil phase and provide a density difference between the oil and inorganic contaminants (e.g.,

water and solid).[11,16,18] However, adding these diluents can lead to asphaltene destabilization in the oil phase, resulting in an engineering optimization problem.

Previous studies have investigated the kinetic precipitation of asphaltenes using conventional light to heavy crude oils, with asphaltene fractions below 11 wt% and without the presence of inorganic solids.[2–4,7,19–21] A larger size and higher mass of precipitated asphaltenes were observed as a function of time using optical microscopy and centrifugation-based separation techniques.[2–4,7,19–21] These results demonstrate that asphaltene precipitation is a kinetic aggregation process. Failure to consider the slow kinetic precipitation process can lead to inaccurate asphaltene solubility and stability measurements. In this work, "kinetic precipitation of asphaltenes" refers to the observation that the total mass separated by centrifugation as a function of time increases as the quantity and size of precipitated asphaltenes grows. Asphaltene precipitation can take several weeks or months to be detected at low diluent concentrations, ≤50 vol% n-heptane in crude oils, provided slow precipitation kinetics occur.[2–4,7,19–21] In this work, the kinetic precipitation of asphaltenes was investigated using bitumen samples, which contains higher asphaltene fractions than previous studies and also have dispersed inorganic solids.[2–4,7,19–21]

Without the presence of seeds (i.e., surfaces or interfaces), self-nucleation or homogeneous nucleation occurs when nuclei form uniformly in the parent phase.[22,23] However, inorganic solids are normally present in bitumen, at a concentration typically on the order of 10 wt%.[11–17] When seeds are present, nuclei can form on the surface of seeds, and this process is called heterogeneous nucleation.[22,23] The energy barrier for phase transition occurring during heterogeneous nucleation is lower than in homogeneous processes because of reduced surface energy required to form a new phase on the surface of a nucleation site.[22] In this work, the term "homogeneous aggregation" means self-

nucleation and aggregation of asphaltenes. The term “heterogeneous nucleation” refers to the asphaltene precipitation process that occurs on solid surfaces. The heterogeneous nucleation process may occur when asphaltene molecules, nanoaggregates, or clusters of nanoaggregates in the solution adhere to a solid interface. As will be demonstrated in this study, when solids are present, both the homogeneous aggregation and heterogeneous nucleation mechanisms need to be considered.

Previous work has used various techniques to investigate asphaltenes that adsorbed on solid surfaces, such as transmission electron microscopy (TEM) equipped with an energy-dispersive X-ray diffraction (EDX) detector,[24,25] Nuclear magnetic resonance spectroscopy (NMR),[24] UV depletion detection,[26,27] X-ray powder diffraction (XRD),[28–31] and a quartz crystal microbalance with dissipation (QCM-D).[32] The surface of solid particles, such as kaolinite,[24,26,28,29,33–35] illite,[24,26,28,29,34] montmorillonite,[28] chlorite,[28] and gold,[32] has been previously shown to have an affinity for the adsorption of polar and aromatic compounds, including asphaltenes.[24–29,32–34] It is well documented that asphaltenes as individual molecules or aggregates can adsorb on surfaces.[36–39] Asphaltene adsorption depends on numerous factors, including asphaltene chemical, structural, and source characteristics,[26,40] total solid surface area,[30] surface chemical and physical properties,[26,40] and crude oil solvency.[27,40] For example, larger total surface area of solids adsorbs higher masses of asphaltenes,[30] higher molecular weight asphaltenes tend to preferentially adsorb on surfaces,[26] and increasing the solvent strength decreases adsorption.[40] Thus, the interaction of asphaltenes with solid interfaces is expected to alter the precipitation process. The terminology adopted in this study differentiates between adsorption, the spontaneous process occurring without a bulk phase transition, and heterogeneous nucleation, the process where a bulk phase transition is assisted by a solid

interface. In this study, the kinetic precipitation of asphaltenes as a function of solid content, solvation strength, and petroleum source was investigated.

Asphaltene aggregation modeling without the presence of inorganic solids has been investigated using a geometric population balance model, PMB, which is based on the Smoluchowski equation.[3,21] The previously applied PBM simulates the growth of asphaltene aggregates from the nanometer to micrometer size by modelling the aggregation of two asphaltene monomers to form a dimer, and so on.[3,21] The aggregation process continues until larger particles are formed and the model is validated by experimental measurements of the separated centrifuged mass. At each step of aggregation, the model fundamentally assumes a second order reaction where the aggregation rate depends on the two colliding particle concentrations and each pair of colliding species have a different rate constant.[3,21,41] Previous work[3,21] has also shown that the model results are in close agreement with experimental data using various diluent types (e.g., n-alkanes) and concentrations. The results have suggested that a PBM model is appropriate to simulate the asphaltene precipitation process without inorganic solids. However, studies that investigated heterogeneous adsorption or deposition generally have a less defined modelling approach. Asphaltene adsorption occurs spontaneously while asphaltene deposition is induced when a bulk phase transition occurs, such as adding heptane into an oil solution. Previous work has investigated asphaltene deposition on different surfaces: stainless steel beads,[42] capillary pipes,[2,3,39] and polymers.[43] It was found that asphaltene deposition could be explained using a diffusion-limited model,[3,39,42,43] and this conclusion provides a pathway for a heterogeneous precipitation mechanism to be modelled. In this investigation, a combined homogeneous aggregation and heterogeneous nucleation model was developed to study the rate precipitation of asphaltene as a function of solid content.

The objective of this work is to investigate the impact of solids on the kinetic precipitation of asphaltenes. Asphaltene precipitation was monitored as a function of time, diluent concentration, and solid content using two types of bitumen samples with naphtha and heptol as diluents. Scanning Electron Microscope with Energy Dispersive X-ray Spectroscopy (SEM-EDS) was applied for investigating solid morphology, elemental component, and specific surface area (SSA). A combined homogeneous aggregation and heterogeneous nucleation model was established to quantify the influence of solid content on the kinetic rate of precipitation of asphaltenes. This investigation leads to a better understanding of asphaltene aggregation in systems with inorganic solids and provides a simple model that can estimate the rate of asphaltene precipitation under different conditions. The conclusions and modeling results are transferable to different geometries and system compositions. Moreover, this work provides a potential new tool to increase the rate of the often-slow kinetic precipitation of asphaltenes using inorganic solids as nucleation sites to reduce experimental time and better purify the bitumen due to larger size of solids and asphaltenes.

4.2 Experimental Methods

4.2.1 Materials

Two types of Athabasca bitumen samples, called BF1 and BF2, were used, which contained different weight fractions of dispersed inorganic solid material. Naphtha (N) and heptol (H, heptane-toluene blends) were used as the diluents (D). Syncrude Canada Ltd. provided bitumen (B) and naphtha (N) samples. High-performance liquid chromatography (HPLC)-grade toluene (T) and n-heptane (C7) were purchased from Fisher Scientific. Various heptol solutions at C7 to toluene volume ratios of 82:18 (H82), 85:15 (H85), 87:13

(H87), and 90:10 (H90) were used. In this study, the D/B ratio is presented by mass ratio and vol%.

4.2.2 Asphaltene Precipitation

A diluent was added to a quantity of bitumen to obtain the desired ratio (by mass), called diluted bitumen. The diluted bitumen was homogenized using a Fisher Scientific™ Model 505 Sonic Dismembrator at 35% amplitude for 4 minutes. The solution was stirred continuously using a magnetic stir bar. Two 10 mL samples were taken using a glass pipette at various times (t_1, t_2, t_3, etc.) and then transferred to two 15 mL centrifuge tubes. The tubes were centrifuged in an Eppendorf centrifuge 5430R using a relative centrifugal force (RCF) of 3,000 g for 10 minutes to separate the precipitated asphaltenes and solids, called the "cake," from the solution. The supernatant was decanted, and a washing solvent, C7, was added to the cake to remove nonasphaltene entrapped oil (i.e., maltenes). The cake with C7 was sonicated using a Branson Ultrasonics 1800 unit for approximately 15 minutes. This washing procedure was continued until the supernatant was a visibly clear solution. The cake was then dried in a vacuum oven (4.9 psi absolute pressure) at 75 °C for approximately 24 h, and the weight of the dry cake that contained precipitated asphaltenes and solids was recorded. The dry cake mass was recorded when the mass was constant as a function of drying time, indicating that all excess n-heptane had been removed. The mass percentage of precipitated asphaltenes and solids, $f_{asp\ and\ solid}$ (g asphaltene precipitated and solids/g bitumen×100%), as a function of time was measured.

After the supernatant was decanted, the cake of some samples contained a quantity of inorganic solids that entrapped oil and soluble asphaltenes along with the precipitated asphaltenes. During the washing step, C7 was added, and it destabilized the soluble

asphaltenes contained within the entrapped oil. These destabilized asphaltenes affect the weight measurement because the mass of asphaltenes precipitated due to the diluent addition and the washing step were measured simultaneously resulting in overestimation of $f_{asp\ and\ solid}$. This observation is called the entrapped oil effect. To obtain the mass of only the precipitated asphaltenes due to the diluent and solids present, $f_{asp\ and\ solid}$, the results need to be corrected. A material balance was developed to estimate the mass of asphaltenes precipitated due to adding C7 during the washing step so that $f_{asp\ and\ solid}$ without the entrapped oil effect could be obtained. Details can be found in the Appendix.

4.2.3 Solid Content Measurement

The original solid content in the bitumen samples was measured using two approaches: toluene/bitumen (T/B) dilution and kinetic sample toluene washing. The solid content measurement using the T/B dilution method used a similar procedure discussed in the Asphaltene Precipitation section, but toluene was used as both the diluent and the washing solvent. The experiments were performed twice at a T/B ratio of 3.4 (80 vol% toluene), and the solution was homogenized using a Fisher Scientific™ Model 505 Sonic Dismembrator at 35% amplitude for 160 seconds. A solution was taken after 24 hours of mixing time with the toluene. This T/B procedure in this study is similar to previous work to measure the solids content of bitumen samples.[44] In the kinetic sample toluene washing approach, approximately 50 dried cake samples from the Asphaltene Precipitation experiments were washed twice with 10 ml toluene. This process dissolved asphaltenes from the cake, and after centrifugation for 10 minutes at 3,000 g and decanting the supernatant, only the solids remained in the tube. In both methods, the weight of the solids

was measured after drying in the oven and the mass percentage of solids, f_{solid} (g solid/g bitumen × 100%), was obtained.

The mass percent of solids, f_{solid}, was used to calculate the precipitated asphaltene mass percent, f_{asp}, by $f_{asp} = f_{asp\ and\ solid} - f_{solid}$. Thus, the quantity of asphaltenes precipitated, f_{asp}, as a function of time at different conditions was obtained. Moreover, the equilibrium mass percent of asphaltenes precipitated at long times, $f_{asp,eq}$, was obtained by averaging f_{asp} values after f_{asp} remained constant as a function of time from mixing the oil with the diluent.

4.2.4 Solids Removal

The effect of solid content on the kinetic precipitation rate of asphaltenes from bitumen was investigated by varying the quantity of solids in the diluted bitumen. To accomplish this task, bitumen samples were pretreated to partially or near completely remove solids before performing the Asphaltene Precipitation experiments. For partial solid removal, bitumen samples were mixed with a diluent to obtain a D/B ratio of 0.5 and the solution was centrifuged for 10 minutes at a RCF of 3,000 g. The supernatant was extracted, and more diluent was added to the supernatant to reach the desired ratio for the Asphaltene Precipitation experiments. In the near complete solid removal approach, bitumen samples were also mixed with a diluent to obtain a D/B ratio of 1, and the solution was centrifuged for 3 h at an RCF of 7,200 g. Again, the supernatant was extracted and further diluted to the desired concentration. The solid content that remained in the solution after the pretreatment procedure was measured using the kinetic sample toluene washing approach, which is discussed in Solid Content Measurement section.

4.2.5 Scanning Electron Microscopy With Energy-Dispersive X-ray Spectroscopy, SEM-EDS, for Solid Investigation

The properties of the inorganic solids were investigated to determine the morphology, elemental component, and specific surface area (SSA) using a Helios NanoLab™ 650 scanning electron microscope with energy-dispersive X-ray spectroscopy. A similar approach as in the Asphaltene Precipitation experiment was used to prepare solid samples, but n-heptane was added into bitumen samples at a ratio of 40:1 (wt%). Two 10 mL samples were taken and centrifuged for 3 h at a RCF of 3,000 g. The cake, which consists of precipitated asphaltenes and solids, was washed with n-heptane and dried. Another solid sample was taken from the dry cake samples that contained precipitated asphaltenes and solids in Asphaltene Precipitation experiments. Both of the dry cake samples from two preparation methods were washed with toluene to dissolve the precipitated asphaltenes using the same approach in Asphaltene Precipitation experiment. The solid samples were then mixed with 5 mL toluene and sonicated for 2-3 minutes to disperse solids and dropped on a strip of copper tape for imaging with the SEM.

4.2.6 A Combined Homogeneous Aggregation and Heterogeneous Nucleation Model

The purpose of the model was to investigate the rate of asphaltene precipitation as a function of solid content and solvent quality (diluent types and concentrations). An experimental data set from the Asphaltene Precipitation experiments was used to tune the model, and then model predictions were compared to a second data set. A faster rate of asphaltene precipitation in the experiments is defined as when the observed mass separated at a fixed time from mixing with a diluent is greater compared to another sample. The precipitation model provides quantitative values of the total, homogeneous, and

heterogeneous precipitation rates.

Homogeneous aggregation rate, r_{ho} [mol/(m^3 s)], was modeled as a single second order reaction, $-r_{ho} = k_{ho}C_A^2$, based on a simplification of a population balance model (PBM)[3,21]. The variable C_A [mol/m^3] is defined as the concentration of asphaltenes in the diluted bitumen that has been destabilized, but has not been separated from the mixture. A single reaction and rate constant of the homogeneous aggregation, k_{ho} [m^3/(mol s)], is assumed unlike in the PBM where multiple simultaneous reactions occur with rate constants varying for each pair of aggregate sizes. The homogeneous rate constant, k_{ho}, is expected to be a function of diluent type and concentration. The rate of heterogeneous nucleation, $-r_{he}$ [mol/(m^3 s)], was modeled as a first order reaction, $-r_{he} = k_{he}C_A$, based on diffusion limited deposition[3,39,42,43]. Details on the first order reaction derivation are in the Appendix. The rate constant of heterogeneous nucleation is k_{he} [1/s] and is written by $k_{he} = \frac{D}{\delta}\frac{A}{V} = k_m \emptyset_b \rho_b S\ (f_{solid})$ where D [m^2/s] is the diffusivity, δ [m] is the boundary layer thickness, A [m^2] is the solid surface area, V [m^3] is the total solution volume, $\emptyset_b$ is the volume fraction of bitumen, ρ_b [g/m^3] is density of bitumen, S (m^2/g) is the specific surface area, and $k_m = \frac{D}{\delta}$ [m/s] is the mass transfer coefficient. When inorganic solids are present, the model allows for asphaltenes to precipitate both homogeneously and heterogeneously. The total rate of asphaltene precipitation, $\frac{dC_A}{dt}$ [mol/(m^3 s)] is written by:

$$\frac{dC_A}{dt} = r_{ho} + r_{he} = (-k_{ho}C_A^2) + (-k_{he}C_A) \quad (1)$$

From eq. **(1)**, C_A as a function of time can be obtained by integration and the end result is shown below. The details of the derivation can be found in the Appendix.

$$C_A = \frac{k_{he}}{k_{ho}}\left\{\left(1 + \frac{k_{he}}{k_{ho}C_{A_0}}\right)e^{-k_{he}t} - 1\right\} \quad (2)$$

The maximum concentration of unstable asphaltenes that precipitate from the solution, C_{A_0} [mol/m^3], is obtained from the Asphaltene Precipitation experiments and depends on the diluent type and concentration. Values of C_{A_0} are determined by $C_{A_0} = \frac{(f_{asp,eq}/100)\times\emptyset_b\times\rho_b}{MW_{asp}}$, where MW_{asp} is an asphaltene nanoaggregate molecular weight, ρ_b is the density of bitumen (assumed as 1000 kg/m^3, and $\emptyset_b$ is the volume fraction of bitumen. The molecular weight of asphaltenes is in the range of 500-7,500 g/mol from molecules to nanoaggregate, and asphaltene nanoaggregates have 4-10 monomers.[45] The asphaltene nanoaggregates are assumed to be the structures that aggregate and influence the rate of asphaltene precipitation. In this study, MW_{asp} is assumed to be 2,000 g/mol, which is the possible minimum value. From the model in eq. (2), if k_{ho} and k_{he} are known, the simulated results of C_A as a function of time can be determined and converted to the mass percent of asphaltenes precipitated from the diluted bitumen, $f_{asp} = f_{asp,eq} - \left(\frac{C_A\times MW_{asp}\times 100\%}{\emptyset_b\times\rho_b}\right)$. The experimental values of mass percent of asphaltenes precipitated, f_{asp}, as a function of time were used to fit the precipitation rate constants.

For the conditions where there were no inorganic solids, k_{he} was fixed at a value sufficiently low, 10^{-10} [1/s], as to effectively eliminate the heterogeneous precipitation mechanism. The k_{ho} that resulted in the minimum sum square error (SSE), which is the summation of the squared difference between the predicted and experimental results, was selected as the best fit. When solids were present, the previously determined k_{ho} was held at a constant value for the same diluent type and concentration. The heterogeneous rate constant, k_{he}, was then varied and at the minimum SSE, k_{he} (and subsequently k_m) was

obtained.

The model was applied to experiments performed with different diluent types and concentrations, bitumen samples, and solid contents. Asphaltene aggregation processes, such as onset time and collision efficiency, have been previously related to the reciprocal of the difference between the asphaltene and surrounding liquid Hildebrand solubility parameters squared, $1/(\delta_{asp}-\delta_{solution})$.[3,20,46,47] The onset time is defined as the time when particle sizes reach 0.5 μm as detected using optical microscopy, and the collision efficiency refers to the probability of an asphaltene collision resulting in adhesion event using a PBM.[3,20,21,46,47] Following the approach of previous work, a relationship between k_{ho} and $1/(\delta_{asp}-\delta_{solution})^2$, was established from the model fits. This relationship was used to estimate k_{ho} as a function of solvent quality, which is a function of diluent type and concentration. The experimental and simulated f_{asp} values as a function of time are directly compared. The combined homogeneous aggregation and heterogeneous nucleation model provides quantitative values for the rate of asphaltene precipitation with and without solids.

4.3 Results and Discussion

The experimental results of the Solid Content Measurement using the T/B dilution method and the kinetic sample toluene washing approach are shown in Table 4.1. Both methods produced similar solids contents results within experimental uncertainty. In this study, the original solid contents for BF1 and BF2 are reported as 1.32% and 0.66%,

Table 4.1 Solid content (wt%) in the bitumen samples.

Bitumen samples	Solid content (wt%)	
	T/B dilution method	Kinetic sample toluene washing approach
BF1	1.32±0.08	1.22±0.13
BF2	0.66±0.04	0.65±0.14

respectively, following the T/B dilution approach measured value.

Figure 4.1 shows the experimental results of mass percent of precipitated asphaltenes as a function of time along with the model fits at minimum SSE between the experimental data (points) and simulated results (dashed line) using H82/BF2 mixtures at diluent ratios of 3.8, 5.7, 7.6, and 9.5 (84.20, 88.88, 91.42, and 93.02 vol% H82) with 0.66% and 0% solid contents. At every D/B ratio performed, the mass percent of precipitated asphaltenes at the 0.66% solid content had a higher value than that at the 0% solid content during the early experimental times (0 to 2 hours). The results reveal that the rate of asphaltene precipitation increases with higher solid content. At sufficiently high solid contents, there was no or difficult to detect kinetic precipitation of asphaltenes. As the D/B ratio is increased, the impact of the solid content because less pronounced due to

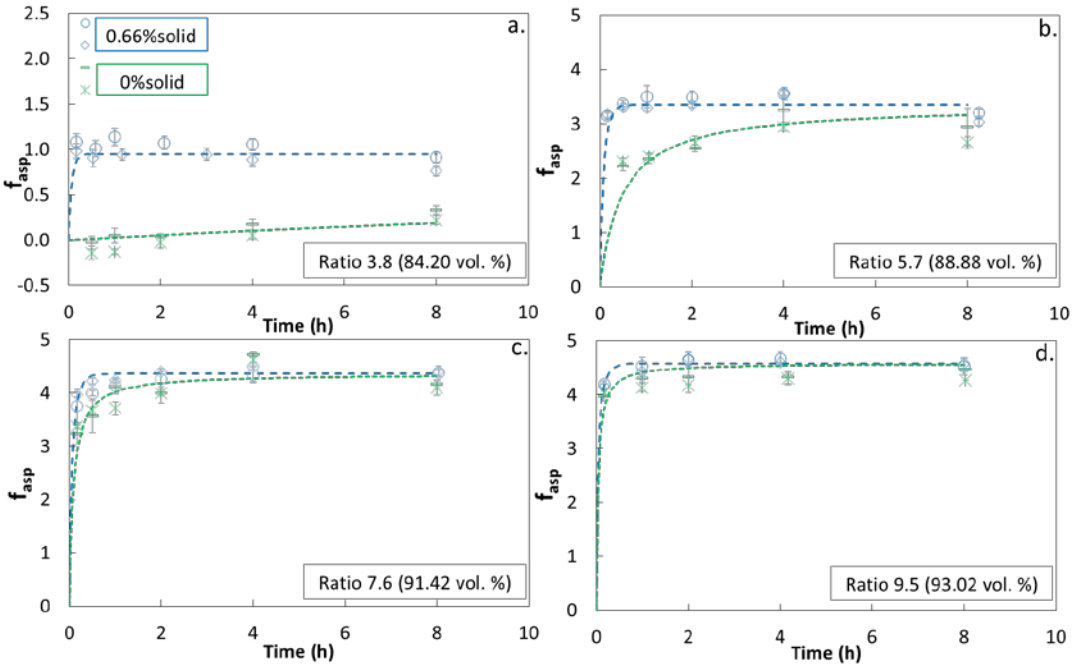

Figure 4.1 The mass percentage of precipitated asphaltenes as a function of time (points) and model fits (dashed line) using H82/BF2 solutions at diluent ratios of a.) 3.8 (84.20 vol%), b.) 5.7 (88.88 vol%), c.) 7.6 (91.42 vol%), and d.) 9.5 (93.02 vol%) with 0.66% and 0% solid content. The experiments were performed twice, and results are indicated using two marker styles.

an increase in the homogeneous aggregation rate, as will be discussed below. The equilibrium mass percent of asphaltenes precipitated increases with increasing D/B ratio as shown in Table 4.2, which is in good agreement with previous work[3,4,7,19]. The results demonstrate that at higher D/B ratios, the solvent strength of the diluted bitumen is reduced and both the mass of precipitated asphaltenes and the rate of their precipitation increase. Values of the equilibrium mass percent of asphaltenes precipitated at the same D/B ratio for different solid contents have similar values, indicating that the presence of the solids does not impact the overall solubility of asphaltenes. The one exception to this observation is for the mixtures at the D/B ratio of 3.8, and Figure 4.1 demonstrates a trend of increasing mass percent of asphaltenes precipitated with time at the 0% solid content. We interpret this observation as asphaltene precipitation having not reached the equilibrium state after 8 hours. Thus, the equilibrium mass percent of asphaltene precipitated for ratio 3.8 between the 0.66% and 0% solid content cannot be compared. However, it is expected that if the experiments were performed for a longer time, the values would be the same. Similar

Table 4.2 The mass of precipitated asphaltenes at equilibrium, $f_{asp,eq}$, at different diluent types and concentrations in BF2 sample for various D/B ratios with 0.66% and 0% solid content.

Solution	Ratio (wt%)	$f_{asp,eq}$ (%)	
		0.66% solid	0% solid
H82/BF2	3.8	0.95±0.20	N/A
	5.7	3.35±0.21	2.79±0.43
	7.6	4.36±0.37	4.25±0.27
	9.5	4.58±0.29	4.29±0.32
H85/BF2	3.8	2.21±0.28	-
H87/BF2	3.8	2.79±0.15	-
H90/BF2	3.8	5.06±0.68	-

equilibrium values between the 0% and 0.66% solid content experiments demonstrate the reliability of the experimental results because the solid content is not expected to influence the asphaltene solubility. The negative mass percent of precipitated asphaltenes at the diluent ratio of 3.8 with 0% solid is likely due to an overcorrection of the entrapped oil procedure and is within the experimental uncertainty. The simulated results (dashed lines) and discussion are provided later in the modeling section below.

The influence of solvent quality on the kinetic precipitation of asphaltenes was investigated at a fixed solid content and H/B ratio, but the ratio of heptane to toluene in the heptol diluent was varied. Figure 4.2 (Left) provides the mass percent of asphaltenes precipitated as a function of time and H ratio in H/BF2 solutions at a diluent ratio of 3.8 with a 0.66% solid content. No kinetic precipitation was observed for the H82 and H90 heptol ratios, and the mass percent of asphaltenes precipitated was approximately constant as a function of time, indicating rapid kinetics of precipitation. Kinetic precipitation was observed using H85 and H87 diluents. An overall faster rate of asphaltene precipitation was observed as the H/B ratio was increased, which agree with the results in

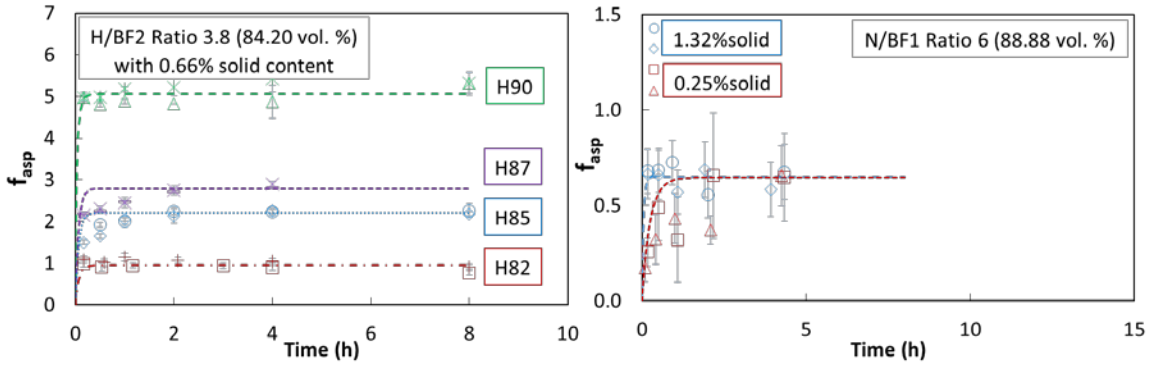

Figure 4.2 The mass percentage of precipitated asphaltenes as a function of time (points) and model fits (dashed line). Left: different H ratios in BF2 at a diluent ratio of 3.8 (84.20 vol%) with 0.66% solid content. Right: N/BF1 solution at a diluent ratio of 6 (88.88 vol%) with 1.32% and 0.25% solid content. The simulated results were calculated using k_{ho} and k_m that were obtained from Figure 4.1.

Figure 4.1 that the decrease in solvent quality increase the rate of asphaltene precipitation. Additional experiments were performed using the BF1 sample and naphtha as the diluent. Figure 4.2 (Right) shows the mass percent of asphaltenes precipitated as a function of time using N/BF1 mixtures at diluent ratios of 6 (88.88 vol%) with the full 1.32% and partially removed 0.25% solid contents. In agreement with the results above, increasing solid contents were found to increase the rate of asphaltene precipitation. The results of Figure 4.2 and Figure 4.1, provide similar trends and demonstrate general applicability of the findings despite the different diluent type and bitumen sample used. These findings support that *both solid content and solvent quality affect the precipitation rate of asphaltenes*. The details of the simulated results (dashed lines) are presented in the modeling section. Numerical values of the equilibrium mass percent of asphaltenes precipitated in Figure 4.2 are also presented in Table 4.2.

Figure 4.3 shows SEM images of the inorganic solids extracted from the BF1 and BF2 sample. The solid morphologies observed were similar with kaolinite in published SEM images of Athabasca clay minerals.[48] Previous work has reported the specific surface area, SSA, of kaolinite to range between 8-21 m^2/g,[12,30,49–52] and in this study the SSA was

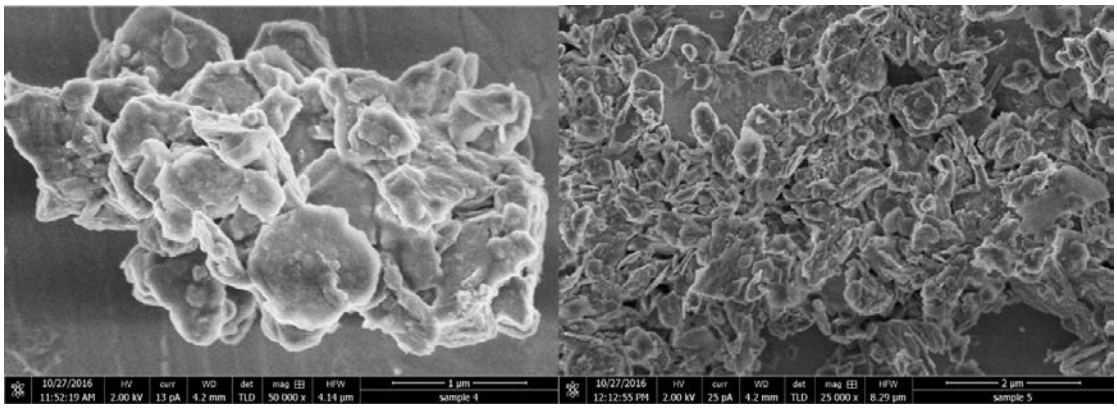

Figure 4.3 SEM images of solids in bitumen samples. Left: Solid from C7:B solution at the diluent ratio of 40:1 method using BF2 sample. Right: Solid from Asphaltene Precipitation experiment using BF1 sample.

estimated to be 8.0 ± 1.9 (Left) and 12.1 ± 3.2 (Right) m^2/g assuming disk shape and a kaolinite density of 2.6 g/cm^3.[53] The details of the SSA estimation procedure are provided in the Appendix. The Al:Si atomic ratio of the solids was measured using EDS and was found to be 2:1.4 (Left) and 2:2.5 (Right), which is similar to the Al:Si ratio found in kaolinite, 2:2. The visual morphology, elemental composition, and SSA estimate suggest that the solids in this investigation were predominantly kaolinite.

The rate and mechanisms of asphaltene precipitation were investigated using the combined homogeneous aggregation and heterogeneous nucleation model. Figure 4.1 provides the model fits superimposed on the measured results of the mass percent of asphaltene precipitated as a function of time, diluent concentration, and solid content for H82/BF2 dilutions. The model results demonstrate a good fit with the experimental measurements, and values of k_{ho} and k_{he} for the results in Figure 4.1 are estimated and provided in Table 4.3. It was observed that k_{ho} increases with increasing D/B ratio, demonstrating that the model can quantify the experimentally observed faster rate of homogenous asphaltene precipitation as the D/B ratio is increased. A single value of k_m=

Table 4.3 Numerical values of k_{ho} and k_{he} as a function of diluent type, concentration, and solid content for experiments using H/BF2 mixtures.

Solution	Ratio (wt%)	$\boldsymbol{k_{ho}}$ (m3/(mol s))	$\boldsymbol{k_{he}}$ (1/s)	Note
H82/BF2	3.8	9.0×10^{-6}	4.1×10^{-3}	From a comparison of simulated and experimental data at the minimum SSE
	5.7	2.5×10^{-4}	2.9×10^{-3}	
	7.6	1.4×10^{-3}	2.3×10^{-3}	
	9.5	3.6×10^{-3}	1.8×10^{-3}	
H85/BF2	3.8	7.1×10^{-5}	4.1×10^{-3}	From the relationship between k_{ho} and $1/(\delta_{asp}-\delta_{solution})^2$ and fitting k_m
H87/BF2	3.8	2.8×10^{-4}	4.1×10^{-3}	
H90/BF2	3.8	2.0×10^{-3}	4.1×10^{-3}	

5.0×10^{-9} m/s is able to accurately model the precipitation rate of asphaltenes with solids present, and the calculated values of k_{he} that vary based on the solid content are reported in Table 4.3. The decrease in k_{he} as the D/B ratio increases is explained by a dilution effect.

The results in Figure 4.1 for the H82/BF2 mixtures were used to estimate k_{ho} and k_{he}, and the predictive capabilities of the model were tested on the results in Figure 4.2, which had different diluent types and concentrations, bitumen samples, and solid contents. In Figure 4.2, experiments at 0% solid content were not performed and k_{ho} could not be determined directly. To estimate k_{ho} values, a relationship between k_{ho} and $1/(\delta_{asp}-\delta_{solution})^2$ was developed for the H82/BF2 precipitation experiments. A correlation function, determined directly. To estimate k_{ho} values, a relationship between k_{ho} and $1/(\delta_{asp}-\delta_{solution})^2$ was developed for the H82/BF2 precipitation experiments. A correlation function, $k_{ho} = 2 \times 10^{19}\left\{\exp(-9.772 \times \frac{10^8}{(\delta_{asp}-\delta_{soultion})^2})\right\}$, was found to fit the measured values appropriately, and this relationship was use to estimate k_{ho} under different experimental conditions, with values of δ_{asp} = 20100, δ_B = 18250, and δ_N = 15500 $Pa^{0.5}$ as determined from previous work[54–56]. Using the correlation, k_{ho} values were calculated for the H/BF2 and N/BF1 experiments and the model fits are presented in Figure 4.2. The values of k_{ho} for the H/BF2 mixtures (Figure 4.2 (Left)) were reported in Table 4.3 and the k_{ho} value for the N/BF1 solutions (Figure 4.2 (Right)) was 1.9×10^{-4} $m^3/(mol\ s)$. The same value of k_m previously obtained was still held constant at 5.0×10^{-9} m/s. Using this approach, the kinetic precipitation model demonstrated accuracy to represent the experiments presented in Figure 4.2 despite the difference in the bitumen source, diluent concentration, and diluent type. The results suggest that the model is reliable and appropriate to investigate and predict the kinetic precipitation of asphaltenes at various solid contents, diluent types

and concentrations, and source bitumen samples.

The appropriateness of the fitted kinetic heterogeneous nucleation parameter, k_m, was investigated by order-of-magnitude analysis. The diffusivity, D, of soluble asphaltenes in toluene has been measured previously with DOSY-NMR and ranges between, 3×10^{-11} and 3.5×10^{-10} m^2/s depending on the asphaltene concentration.[56–58] However, insoluble asphaltenes are what is precipitating in this study, and lower D values than previous work[56–58] on fully soluble asphaltenes are expected. Assuming a spherical shape for insoluble asphaltenes and using the Stokes-Einstein equation with D = 10^{-13}-10^{-12} m^2/s and 30 Pa s for bitumen viscosity,[59] the hydrodynamic radius of asphaltenes can be estimated to be 0.1-2.4 μm. These values are reasonable due to the expected larger hydrodynamic radius of precipitating asphaltenes compared to the soluble asphaltene value of 0.002 μm measured previously using DOSY NMR[58]. From $k_m = \frac{D}{\delta}$ (detail in Appendix), for D values ranging between 10^{-13} and 10^{-12} m^2/s, the boundary layer thickness, δ, was estimated to be between 2 to 20 μm, which seems reasonable because the radius of solids was also in the micron range, 0.1-0.6 μm from SEM images. The maximum asphaltene thickness, l [μm], on the solid surfaces was calculated assuming that all insoluble asphaltenes precipitated following the heterogeneous mechanism. The asphaltene thickness was estimated from $l = \frac{V_{asp}}{A} = \frac{f_{asp}/\rho_{asp}}{f_{solid} \times S}$ assuming $\rho_{asp} = 1.2$ g/cm^3. Table 4.4 shows the calculated asphaltene thickness as a function of bitumen source, diluent concentration, diluent type, and solid content. The results demonstrate the predictable conclusions that asphaltene thickness increases with a higher mass of precipitating asphaltenes or lower solid content. The range of the asphaltene thickness was found to be 0.02 to 0.8 μm, which are in the same order of magnitude of radius of solids from SEM images and calculated hydrodynamic radius of asphaltenes.

Table 4.4 The calculated asphaltene thickness as a function of bitumen source, and diluent concentration, diluent type, and solid content.

Diluent	Bitumen	Ratio	f_{solid}	Maximum asphaltene thickness (μm)	
				S=8.0±1.9 m^2/g	S=12.1±3.2 m^2/g
H82	BF2	3.8	0.66	0.15±0.05	0.10±0.04
H82	BF2	5.7	0.66	0.53±0.17	0.35±0.12
H82	BF2	7.6	0.66	0.69±0.22	0.45±0.16
H82	BF2	9.5	0.66	0.73±0.23	0.48±0.17
H85	BF2	3.8	0.66	0.35±0.11	0.23±0.08
H87	BF2	3.8	0.66	0.44±0.14	0.29±0.10
H90	BF2	3.8	0.66	0.80±0.25	0.53±0.19
N	BF1	4	1.32	0.03±0.01	0.02±0.01
N	BF1	4	0.25	0.16±0.05	0.10±0.04
N	BF1	6	1.32	0.05±0.02	0.03±0.01
N	BF1	6	0.25	0.27±0.09	0.18±0.06

These order of magnitude results suggest that k_m obtained in this study is within reasonable ranges based on the modeling assumptions.

The simulated and experimental results demonstrate that the asphaltene precipitation process depends on the rates of the heterogeneous and homogeneous precipitation mechanisms. The rates, r_{ho} and r_{he}, were calculated from experiments performed at various H ratios in BF2 at ratio a diluent ratio of 3.8 with the 0.66% and 0% solid contents. The rates depend on time, but in Table 4.5 the results at the initial time, <0.01 h, are shown for the purpose of discussion. The rate of heterogeneous nucleation was observed to be upwards of 500 times faster than the rate of homogeneous aggregation. However, as the solvent strength decreased and the quantity of precipitating asphaltenes increased, the rate of homogeneous aggregation could exceed that of heterogeneous nucleation.

The kinetic precipitation of asphaltene results can be divided into 2 categories based on the experimental conditions: Figure 4.4 (Left): Varying solid content at fixed solvent

Table 4.5 Numerical values of r_{ho} and r_{he} using various H ratios in BF2 at ratio a diluent ratio of 3.8 at 0.01 h.

Solution	$f_{asp,eq}$ (%)	r_{ho} mol/(m^3 s))	r_{he} mol/(m^3 s))	$\frac{dC_A}{dt}$ (mol/(m^3 s))	
		0.66% and 0% solid	0.66% solid	0% solid	0.66% solid
H82/BF2	0.95±0.20	5.9×10^{-6}	3.3×10^{-3}	5.9×10^{-6}	3.4×10^{-3}
H85/BF2	2.21±0.28	2.4×10^{-4}	7.7×10^{-3}	2.4×10^{-4}	7.9×10^{-3}
H87/BF2	2.79±0.15	1.5×10^{-3}	9.4×10^{-3}	1.5×10^{-3}	1.1×10^{-2}
H90/BF2	5.06±0.68	2.1×10^{-2}	1.3×10^{-2}	2.1×10^{-2}	3.3×10^{-2}

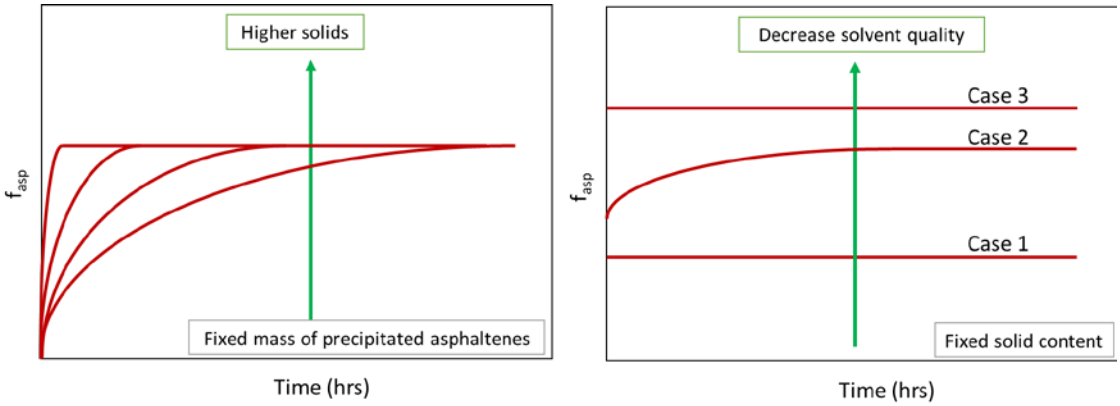

Figure 4.4 Possible results of kinetic precipitation of asphaltenes with different solid contents and mass of precipitated asphaltenes in the solution.

power (constant mass of precipitated asphaltenes), and Figure 4.4 (Right): Fixed solid content while varying solvent power (varying mass of precipitated asphaltenes).

In Figure 4.4 (Left), increasing the concentration of solids increases the rate of heterogeneous asphaltenes precipitation, resulting in an overall faster rate of asphaltene precipitation. At sufficiently high solid content the rate of precipitation is fast enough so that no kinetic effects are observed. The definition of what quantity of solids represents a "high" solid content depends on the solvent power, which is a function of bitumen source, diluent type, and diluent concentration. The rate of asphaltene precipitation also depends on the solvency power of the diluted bitumen mixture, which influences the mass of precipitated asphaltenes. At a fixed solid content but with varied solvency power, experiments can be divided into 3 cases, as shown in Figure 4.4 (Right). Case 1 at high

solvent power demonstrates no observable kinetic precipitation of asphaltenes. In this case, a low mass of asphaltene precipitate and the likelihood of asphaltenes encountering a solid interface is greater than encountering another precipitating asphaltene. Consequently, unstable asphaltenes precipitate predominantly following the heterogeneous nucleation mechanism. For case 2**,** a higher mass of asphaltenes precipitates and both the rate of homogeneous aggregation and heterogeneous aggregation increase. Because of the greater quantity of precipitating asphaltenes, kinetic precipitation can be observed. In case 3, the highest mass of asphaltenes precipitate and both homogeneous aggregation and heterogeneous precipitation are rapid. Thus, the fastest rate of asphaltene precipitation is observed in case 3.

The newly observed heterogeneous precipitation mechanism presented in this study has a number of potential impacts on laboratory studies and industrial observations. The developed model shows that the heterogeneous precipitation with the dispersed solids, which in this case is kaolinite, is a function of the surface area, and it is expected that the deposition of asphaltenes on a variety of dispersed solid types should exhibit similar behavior. However, further investigation is recommended and underway. Asphaltene deposition experiments have also previously been performed using a number of surfaces: stainless steel beads,[42] capillary pipes,[2,3,39] and polymers.[43] We suspect that this heterogeneous precipitation mechanism will also be present not only for dispersed solids but also with other surfaces meaning that the developed model is also can be used with other surfaces. However, further studies are suggested because surface properties might also play a role in the heterogeneous mechanism. Moreover, a potential new tool to increase the rate of the often-slow kinetic precipitation of asphaltenes using inorganic solids as nucleation sites to remove unstable asphaltenes is potentially possible. At low precipitant

concentration, asphaltene precipitation can take weeks to reach equilibrium.[2,3,7,19,20,60] Removing the kinetic effect can help in measuring the asphaltene solubility at low concentrations, which is a significant barrier to generate accurate data to develop thermodynamic models to investigate and understand asphaltene precipitation. For the production perspective, eliminating kinetics can help removing unstable asphaltenes at the beginning of production, which could reduce asphaltene precipitation and deposition problems. However, the solids can increase the corrosion issues meaning that asphaltene and corrosion problems should be considered simultaneously if inorganic solids are used.

4.4 Conclusion

The rate of asphaltene precipitation is affected by dispersed inorganic solids following the discovered heterogeneous precipitation mechanism. A heterogeneous and homogeneous precipitation model was developed, and the results provide accurate fits to the experimental results as a function of the bitumen source, diluent type, diluent concentration, and solid content. Under most circumstances, the rate of heterogeneous nucleation was observed to be faster than the rate of homogeneous aggregation, but as the solvent strength decreased, homogeneous aggregation could become the dominant mechanism. This finding can lead to a potential new tool to increase the rate of the often-slow kinetic precipitation of asphaltenes using inorganic solids as nucleation sites to remove unstable asphaltenes. As a result, the asphaltene problems during the production could be reduced and the essential solubility data for modeling the phase behavior of asphaltenes could conveniently be obtained.

4.5 References

(1) Cimino, R.; Correra, S.; Bianco, A. D.; Lockhart, T. P. *Asphaltene: Fundamentals and Applications*; Springer: New York, 1995; pp 97–130.

(2) Hoepfner, M. P.; Limsakoune, V.; Chuenmeechao, V.; Maqbool, T.; Fogler, H. S. *Energy Fuels* **2013**, *27* (2), 725–735.

(3) Chaisoontornyotin, W.; Haji-Akbari, N.; Fogler, H. S.; Hoepfner, M. P. *Energy Fuels* **2016**, *30* (3), 1979–1986.

(4) Chaisoontornyotin, W.; Bingham, A. W.; Hoepfner, M. P. *Energy Fuels* **2017**, *31* (4), 3392–3398.

(5) Ahmed, H.; John, R. *Asphaltenes, Heavy Oils, and Petroleomics*; Springer: New York, 2007; pp 617–660.

(6) Hoepfner, M. P.; Vilas Bôas Fávero, C.; Haji-Akbari, N.; Fogler, H. S. *Langmuir* **2013**, *29* (28), 8799–8808.

(7) Maqbool, T.; Srikiratiwong, P.; Fogler, H. S. *Energy Fuels* **2011**, *25* (2), 694–700.

(8) Beck, J.; Svrcek, W. Y.; Yarranton, H. W. *Energy and Fuels* **2005**, *19* (3), 944–947.

(9) Hosseini-Dastgerdi, Y.; Tabatabaei-Nejad, S. A. R.; Khodapanah, E.; Sahraei, E. *ASIA-PACIFIC J. Chem. Eng.* **2014**, *10* (1), 1–14.

(10) Alboudwarej, H.; Akbarzadeh, K.; Beck, J.; Svrcek, W. Y.; Yarranton, H. W. *AIChE J.* **2003**, *49* (11), 2948–2956.

(11) Rao, F.; Liu, Q. *Energy Fuels* **2013**, *27* (12), 7199–7207.

(12) Masliyah, J. H.; Czarnecki, J.; Xu, Z. *Handbook on Theory and Practice of Bitumen Recovery from Athabasca Oil Sands Volume I*; Kingsley: Alberta, 2011; Vol. 1, pp 173–256.

(13) Clark, K. A.; Pasternack, D. S. *Ind. Eng. Chem.* **1932**, *24* (12), 1410-14–16.

(14) Tran, F. T.; Couillard, D. *Chem. Prot. Environ.* **1985**, 691–700.

(15) Tran, F. T.; Couillard, D.; Rouleau, D. *Can. J. Chem. Eng.* **1988**, *66* (3), 386–392.

(16) Yang, X.; Czarnecki, J. *Colloids Surfaces A Physicochem. Eng. Asp.* **2002**, *211* (2–3), 213–222.

(17) Czarnecki, J.; Masliyah, J.; Xu, Z.; Dabros, M. *Handbook on Theory and Practice of Bitumen Recovery from Athabasca Oil Sands Volume II*; Kingsley: Alberta, 2013; pp 224–226.

(18) Yang, X.; Hamza, H.; Czarnecki, J. *Energy Fuels* **2004**, *18* (3), 770–777.

(19) Maqbool, T.; Balgoa, A. T.; Fogler, H. S. *Energy Fuels* **2009**, *23* (9), 3681–3686.

(20) Haji-Akbari, N.; Masirisuk, P.; Hoepfner, M. P.; Fogler, H. S. *Energy Fuels* **2013**, *27* (5), 2497–2505.

(21) Maqbool, T.; Raha, S.; Hoepfner, M. P.; Fogler, H. S. *Energy Fuels* **2011**, *25* (4), 1585–1596.

(22) Thanh, N. T. K.; Maclean, N.; Mahiddine, S. *Chem. Rev.* **2014**, *114* (15), 7610–7630.

(23) Kousaka, Y.; Nomura, T.; Alonso, M. *Adv. Powder Technol.* **2001**, *12* (3), 291–309.

(24) Kotlyar, L. S.; Sparks, B. D.; Woods, J. R.; Chung, K. H. *Energy Fuels* **1999**, *13* (2), 346–350.

(25) Bensebaa, F.; Kotlyar, L. S.; Sparks, B. D.; Chung, K. H. *Can. J. Chem. Eng.* **2000**, *78* (August), 610–616.

(26) Dudášová, D.; Simon, S.; Hemmingsen, P. V.; Sjöblom, J. *Colloids Surfaces A Physicochem. Eng. Asp.* **2008**, *317* (1–3), 1–9.

(27) Mendoza de la Cruz, J. L.; Castellanos-Ramírez, I. V.; Ortiz-Tapia, A.; Buenrostro-González, E.; Durán-Valencia, C. de los A.; López-Ramírez, S. *Colloids Surfaces A Physicochem. Eng. Asp.* **2009**, *340* (1–3), 149–154.

(28) Czarnecka, E.; Gillott, J. E. *Clays Clay Miner.* **1980**, *28* (3), 197–203.

(29) Unal, Y.; Kar, T.; Mukhametshina, A.; Hascakir, B. *Proc. - SPE Int. Symp. Oilf. Chem.* **2015**, *2*, 1199–1211.

(30) Kokal, S.; Tang, T.; Schramm, L.; Sayegh, S. *Colloids Surfaces A Physicochem. Eng. Asp.* **1995**, *94* (2), 253–265.

(31) Pernyeszi, T.; Patzkó, Á.; Berkesi, O.; Dékány, I. *Colloids Surfaces A Physicochem. Eng. Asp.* **1998**, *137* (1), 373–384.

(32) Abudu, A.; Goual, L. *Energy Fuels* **2009**, *23* (3), 1237–1248.

(33) Wang, S.; Liu, Q.; Tan, X.; Xu, C.; Gray, M. R. *Energy Fuels* **2013**, *27* (5), 2465–2473.

(34) Pourmohammadbagher, A.; Shaw, J. M. *Energy Fuels* **2016**, *30* (8), 6561–6569.

(35) Wang, S.; Liu, Q.; Tan, X.; Xu, C.; Gray, M. R. *Colloids Surfaces A Physicochem. Eng. Asp.* **2016**, *504*, 280–286.

(36) Zahabi, A.; Gray, M. R.; Dabros, T. *Energy Fuels* **2012**, *26* (2), 1009–1018.

(37) Rudrake, A.; Karan, K.; Horton, J. H. *J. Colloid Interface Sci.* **2009**, *332* (1), 22–31.

(38) Amin, J. S.; Ayatollahi, S.; Alamdari, A. *Appl. Surf. Sci.* **2009**, *256* (1), 67–75.

(39) Nabzar, L.; Aguiléra, M. E. *Oil Gas Sci. Technol.* **2008**, *63* (1), 21–35.

(40) Adams, J. J. *Energy Fuels* **2014**, *28* (5), 2831–2856.

(41) Elimelech, M.; Gregory, J.; Jia, X.; Williams, R. *Particle Deposition and Aggregation: Measurement, Modelling and Simulation*, 1st ed.; Butterworth-Heinemann, Oxford, UK, 1995.

(42) Fávero, C. V. B.; Hanpan, A.; Phichphimok, P.; Binabdullah, K.; Fogler, H. S. *Energy Fuels* **2016**, *30* (11), 8915–8921.

(43) Lin, Y.-J.; He, P.; Tavakkoli, M.; Mathew, N. T.; Fatt, Y. Y.; Chai, J. C.; Goharzadeh, A.; Vargas, F. M.; Biswal, S. L. *Langmuir* **2016**, *32* (34), 8729–8734.

(44) Tharanivasan, A. K.; Yarranton, H. W.; Taylor, S. D. *Energy Fuels* **2012**, *26*, 6869–6875.

(45) Zuo, J. Y.; Mullins, O. C.; Dong, C.; Zhang, D. *Nat. Resour.* **2010**, *1*, 19–27.

(46) Haji-Akbari, N.; Teeraphapkul, P.; Fogler, H. S. *Energy Fuels* **2014**, *28* (2), 909–919.

(47) Haji-Akbari, N.; Teeraphapkul, P.; Balgoa, A. T.; Fogler, H. S. *Energy Fuels* **2015**, *29* (4), 2190–2196.

(48) Zhang, G.; Wasyliuk, K.; Pan, Y. *Can. Mineral.* **2001**, *39* (5), 1347–1363.

(49) Schroth, B. K.; Sposito, G. *Clays Clay Miner.* **1997**, *45* (1), 85–91.

(50) Ibanez, M.; Wijdeveld, A.; Chassagne, C. *Clays Clay Miner.* **2014**, *62* (5), 374–385.

(51) Osacky, M.; Geramian, M.; Ivey, D. G.; Liu, Q.; Etsell, T. H. *Energy Fuels* **2015**, *29* (7), 4150–4159.

(52) Jiang, T.; Hirasaki, G. J.; Miller, C. A. *Energy Fuels* **2010**, *24* (4), 2350–2360.

(53) Gruner, J. W. *Am. Mineral.* **1937**, *22*, 855–860.

(54) Sato, T.; Araki, S.; Ryuzo, M.; Yamamoto, H. *Energy Fuels* **2014**, *28* (2), 891–897.

(55) Barton, A. F. M. *Handbook of Solubility Parameters and Other Cohesion Parameters*; CRC Press: New York, 1991; pp 277–284.

(56) Gray, M. R. *Upgrading Petroleum Residues and Heavy Oils*; The University of Alberta Press Ring: Alberta, 2015; pp 1–15.

(57) Lisitza, N. V; Freed, D. E.; Sen, P. N.; Song, Y. Q. *Energy Fuels* **2009**, *23* (16), 1189–1193.

(58) Durand, E.; Clemancey, M.; Lancelin, J. M.; Verstraete, J.; Espinat, D.; Quoineaud, A. A. *Energy Fuels* **2010**, *24* (2), 1051–1062.

(59) Angle, C. W.; Lue, L.; Dabros, T.; Hamza, H. A. *Energy Fuels* **2005**, *19* (5), 2014–2020.

(60) Wang, J.; Buckley, J. S. *Energy Fuels* **2003**, *17* (7), 1445–1451.

CHAPTER 5

CONCLUSION AND FUTURE WORK

5.1 Conclusion

The findings from this dissertation emphasize the importance of precipitation kinetics and provide ideas and understanding on the behavior of asphaltenes. Chapter 2 shows that the conclusions can be significantly changed from partial to full reversibility of asphaltene precipitation if the kinetic effect is considered. The results indicate that the experimental data used to validate and benchmark the thermodynamic models should be allowed to reach the true equilibrium state, meaning that the kinetic precipitation of asphaltenes needs to be considered. The thermodynamic models can be used to investigate the asphaltene behavior for a full range of operating conditions in the petroleum production, which is unlike experimental methods. In addition, with the inorganic solids as shown in Chapter 4, the rate of asphaltene precipitation can be greatly increased. The usage of inorganic solids to increase the rate of asphaltene precipitation would make obtaining the experimental data at the equilibrium state become easier and more convenient to develop thermodynamic models. Moreover, Chapter 3 demonstrates that thermodynamic properties can possibly be used to predict the time when asphaltenes start depositing and the aggregation process using the relationship of asphaltene deposition, asphaltene aggregation, and thermodynamic driving forces. The deposit growth was demonstrated to be a transport limited deposition process, which can lead to developing a new and more

accurate deposition models. The aggregation process with the presence of solids was successfully modeled based on the finding of a transport limited deposition process. The model can potentially provide the roughly ideas on how to design the bitumen process to eliminate the kinetic precipitation of asphaltenes. Eliminating kinetics using inorganic solids can help removing unstable asphaltenes at the beginning of production, which reduce asphaltene precipitation and deposition problems.

5.2 Future Work

5.2.1 Reversibility of Asphaltene Precipitation in Micro Scale

Asphaltene precipitation is a reversible process while this behavior was investigated on the macro scale, as shown in Chapter 2, it is not clear in the micro scale. The results in the micro scale will reconfirm if the thermodynamic models are appropriate to model the asphaltene phase behavior. On the micro scale, stable and soluble asphaltenes are generally molecule, nanoaggregate, and cluster strutures in the solution ranging size from 1.5 to 5 nm detected by X-ray/Neutron Diffraction and Small-Angle X-ray/Neutron Scattering (SAXS/SANS).[1–5] After a change of pressure, composition, or temperature, stable asphaltenes destabilize and become unstable and insoluble asphaltenes. The sizes of insoluble asphaltenes are >500 nm but due to the limitation of previous techniques, insoluble asphaltene sizes of <40 nm were detected.[4,6] Ultra-Small Angle X-ray Scattering (USAXS) is a recommended technique to detect stable and unstable asphaltenes simultaneously. USAXS is a powerful instrument that can detect and measure the size and shape of asphaltenes from nanometer to micrometer length scale, which is a wider size range than SAXS/SANS.[7,8] Asphaltene solutions, such as crude oil or model oil (asphaltenes in a solvent), will be loaded in the glass capillary tubes which are then sealed.

The temperature will be varied inside the instrument and changes in size and shape of asphaltenes from stable nanoaggregates to unstable asphaltenes can be monitored. The temperature is an easier parameter to be changed inside the instrument compared to composition and pressure changes. If asphaltenes precipitation are a reversible process in the micro scale, the size and shape before and after the change of temperatures should be similar. Moreover, USAXS can be used as a new tool to monitor instantaneous asphaltene destabilization using temperature-induced aggregation. It would be the first time to be able to observe the size and shape of destabilized asphaltenes at the initial time, which provides new knowledge of asphaltene behavior at the initial time.

5.2.2 Asphaltene Deposition Using the Change of Temperature

Asphaltene precipitation induced by changes in composition, pressure, and temperature has been shown by previous work and this work to be a fully reversible process. Asphaltene deposition was investigated using a capillary apparatus, and a precipitant was used to destabilized asphaltenes as shown in Chapter 3 and previous work.[9–14] However, temperature is often an easy experimental parameter to manipulate in the laboratory at atmospheric pressure conditions. Chapter 3 shows that the relationship between the kinetic aggregation process and the deposition detection time with the solubility parameter is present using different precipitant types and concentrations and the deposit growth is a diffusion-limited process. However, only one temperature was tested. Figure 5.1 shows the proposed a capillary apparatus using a change of temperature to destabilize asphaltenes. Asphaltene solutions are kept in the reservoir that is stirred continuously and held at a constant temperature. The different temperatures destabilize different amount of asphaltenes, which change the solubility of asphaltenes in the solution.

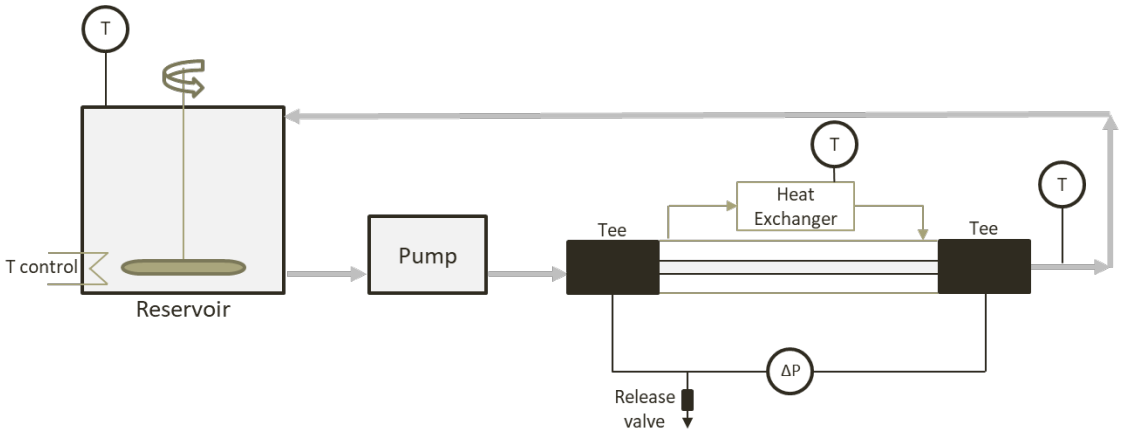

Figure 5.1 Proposed capillary apparatus using the change of temperature to destabilize asphaltenes.

The decreases in temperature decrease the solubility of asphaltenes in the solution. The temperature in the reservoir is held at elevated temperature to ensure that asphaltenes are all soluble in the solution. The solution is fed to the capillary tube using a pump at a specified flow rate. Pressure transducers are located at the beginning and the end of the capillary to measure the pressure drop inside the tube. The capillary tube is designed to be inside of a bigger tube, which acts as a heat exchanger to control the temperature inside the test section of the capillary. The heat exchanger is lower the temperature of the solution inside the capillary tube and asphaltenes deposit on the tube, which can detect by the increase of the pressure drop. The temperature is also measured at the outlet of the capillary tube to measure the change of temperature, and then the solution is fed back to the reservoir. The solution in the reservoir can be heated and flowed through the tube to collect the deposited asphaltenes back to the solution.

In this proposed work, pressure drop at different temperatures can be measured, which can validate the relationship between the kinetic aggregation process and the deposition detection time with the solubility parameter and the diffusion-limited process of deposit growth. If the relationship holds true for all other temperatures, it will help

investigating and understanding the asphaltene aggregation and deposition meaning that by knowing the thermodynamic driving forces at operating temperature, the asphaltene aggregation and the staring deposit time can be easily estimated. Furthermore, if a precipitant was used to destabilize the asphaltenes, more solution is required at a higher flow rate, but in this proposed system the solution can be reused, which allows the experiments to be performed at different flow rates and shear rates. This system allows to test if the growth of deposited asphaltenes is always diffusion limited using different shear rates. Investigation of the thermodynamic driving force that causes this behavior in order to understand asphaltene deposition is also recommended.

5.2.3 Inorganic Solids

Inorganic solids were found to increase the rate of asphaltene precipitation as shown in Chapter 4, but it is not clear what type of solids play the most significant role. In this work, many inorganic solids are present in the samples, and the highest quantity of any single solid type is kaolinite clay.[15] This explanation might be the reason why only kaolinite was found in this work using SEM-EDS. Studying the influence of different inorganic solid types on the kinetic precipitation of asphaltenes is recommended. Samples such as asphaltenes in toluene with different solid types (e.g., kaolinite and illite), which are the solids that are present in the bitumen extraction process,[16] can be used. A precipitant will then added to the samples at a designed precipitant concentration to destabilize the asphaltenes. The mass of precipitated asphaltenes will be measured as a function of time to investigate the rate of asphaltene precipitation. The results can indicate which solid types play the most significant role on the kinetic precipitation of asphaltenes. Moreover, different specific surface areas might also affect the kinetics, and further investigation is

needed. To investigate this effect, one type of solid can be used and the experiment repeated with varied size of solids in the samples. Smaller sized inorganic solid particles at the same overall weight loading will have a greater specific surface area compared to larger particles. These findings will provide more information in designing the conditions such as the type and size of inorganic solids to eliminate kinetics during the production process. For the production perspective, eliminating kinetics can help by removing unstable asphaltenes at the beginning of production, which improves the purification of bitumen during the process. Moreover, at low precipitant concentration, asphaltene precipitation can take weeks to reach equilibrium.[9,17–20] Removing the kinetic effect can help in measuring the asphaltene solubility at low concentrations, which is a significant barrier to generate accurate data to develop thermodynamic models to investigate and understand asphaltene precipitation.

5.3 References

(1) Mullins, O. C.; Sabbah, H.; Pomerantz, A. E.; Andrews, a B.; Ruiz-morales, Y.; Mostow, F.; Mcfarlane, R.; Goual, L.; Lepkowicz, R.; Cooper, T.; Orbulescu, J.; Leblanc, R. M.; Edwards, J.; Zare, R. N.; Barre, L.; Andrews, a B.; Ruiz-morales, Y.; Mostowfi, F.; Mcfarlane, R.; Goual, L.; Lepkowicz, R.; Cooper, T.; Orbulescu, J.; Leblanc, R. M.; Edwards, J.; Zare, R. N. *Energy Fuels* **2012**, *26* (7), 3986−4003.

(2) Mullins, O. C.; Sabbah, H.; Pomerantz, A. E.; Andrews, A. B.; Ruiz-morales, Y.; Mostow, F.; Mcfarlane, R.; Goual, L.; Lepkowicz, R.; Cooper, T.; Orbulescu, J.; Leblanc, R. M.; Edwards, J.; Zare, R. N. *Energy Fuels* **2012**, *26* (7), 3986–4003.

(3) Yen, T. F.; Erdman, J. G.; Pollack, S. S. *Anal. Chem.* **1961**, *33* (11), 1587–1594.

(4) Hoepfner, M. P.; Vilas Bôas Fávero, C.; Haji-Akbari, N.; Fogler, H. S. *Langmuir* **2013**, *29* (28), 8799–8808.

(5) Hoepfner, M. P.; Fogler, H. S. *Langmuir* **2013**, *29* (49), 15423–15432.

(6) Tanaka, R.; Sato, E.; Hunt, J. E.; Winans, R. E.; Sato, S.; Takanohashi, T. *Energy Fuels* **2004**, *18* (7), 1118–1125.

(7) Ilavsky, J.; Zhang, F.; Allen, A. J.; Levine, L. E.; Jemian, P. R.; Long, G. G. *Metall. Mater. Trans. A* **2013**, *44*, 68–76.

(8) Ilavsky, J.; Allen, A. J.; Levine, L. E.; Zhang, F.; Jemian, P. R.; Long, G. G. *J. Appl. Crystallogr.* **2012**, *45* (6), 1318–1320.

(9) Hoepfner, M. P.; Limsakoune, V.; Chuenmeechao, V.; Maqbool, T.; Fogler, H. S. *Energy Fuels* **2013**, *27* (2), 725–735.

(10) Broseta, D.; Robin, M.; Savvidis, T.; Féjean, C.; Français, I.; Durandeau, M.; Zhou, H.; Ep, E. *SPE*; 2000; pp 1–9.

(11) Wang, J.; Buckley, J. S.; Creek, J. L. *J. Dispers. Sci. Technol.* **2004**, *25* (3), 287–298.

(12) Lawal, K. a.; Crawshaw, J. P.; Boek, E. S.; Vesovic, V. *Energy Fuels* **2012**, *26* (4), 2145–2153.

(13) Nabzar, L.; Aguiléra, M. E. *Oil Gas Sci. Technol.* **2008**, *63* (1), 21–35.

(14) Boek, E. S.; Ladva, H. K.; Crawshaw, J. P.; Padding, J. T. *AIP Conf. Proc.* **2008**, *1027* (4), 273–275.

(15) Masliyah, J. H.; Czarnecki, J.; Xu, Z. *Handbook on Theory and Practice of Bitumen Recovery from Athabasca Oil Sands Volume I*; Kingsley: Alberta, 2011; Vol. 1, pp 173–256.

(16) Gray, M. R. *Upgrading Petroleum Residues and Heavy Oils*; The University of Alberta Press Ring: Alberta, 2015; pp 1–15.

(17) Maqbool, T.; Srikiratiwong, P.; Fogler, H. S. *Energy Fuels* **2011**, *25* (2), 694–700.

(18) Wang, J.; Buckley, J. S. *Energy Fuels* **2003**, *17* (7), 1445–1451.

(19) Maqbool, T.; Balgoa, A. T.; Fogler, H. S. *Energy Fuels* **2009**, *23* (9), 3681–3686.

(20) Chaisoontornyotin, W.; Haji-Akbari, N.; Fogler, H. S.; Hoepfner, M. P. *Energy Fuels* **2016**, *30* (3), 1979–1986.

APPENDIX

SUPPORTING INFORMATION

A.1 Material Balance on the Asphaltene Cake

A material balance was developed to estimate the mass of precipitated asphaltenes due to adding C7 in the washing step, $m_{asp,wash}$, so that $f_{asp\ and\ solid}$ without the entrapped oil effect was obtained. Due to the entrapped oil in precipitated asphaltenes and solids, adding n-heptane during the washing step of the Asphaltene Precipitation experiments leads to additional precipitated asphaltenes. These precipitated asphaltenes increase the $f_{asp\ and\ solid}$ measurement meaning that the $f_{asp\ and\ solid}$ needed to be corrected to obtain accurate $f_{asp\ and\ solid}$ values without the mass of precipitated asphaltenes formed during the n-heptane washing. In order to eliminate the precipitated asphaltenes due to adding n-heptane, a material balance was used as shown below. It is defined that the mass of wet cake is mass of the cake after the solution was centrifuged and supernatant was decanted, $m_{wet\ cake}$;

$$m_{wet\ cake} = m_{entrapped\ oil} + m_{solid} + m_{asp,D} \tag{S3}$$

Where $m_{entrapped\ oil}$ is the mass of entrapped oil in wet cake, m_{solid} is the mass of solids in wet cake, and $m_{asp,D}$ is the mass of precipitated asphaltenes due to the addition of a diluent. The mass of precipitated asphaltenes due to adding n-heptane in the washing step, $m_{asp,C7}$ can be estimated using

$$m_{asp,C7} = f_{asp,C7} \times \emptyset_B \times V_{D/B} \times \rho_B \quad \text{(S4)}$$

$$V_{D/B} = \frac{m_{entrapped\ oil}}{\rho_{D/B}} \quad \text{(S5)}$$

Where $f_{asp,C7}$ is the mass percentage of precipitated asphaltenes due to heptane addition, $\emptyset_B$ is the volume fraction of bitumen in diluted mixture, $V_{D/B}$ is the total volume of entrapped oil, ρ_B is the density of bitumen (1 g/cm^3), and $\rho_{D/B}$ is the density of the D/B solution. The density values of heptane, toluene, and naphtha were 0.68, 0.86, and 0.75 g/cm^3, respectively. From equation (S4) and (S5), $m_{entrapped\ oil}$ can be identified as shown below.

$$m_{entrapped\ oil} = \frac{m_{asp,C7} \times \rho_{D/B}}{f_{asp,C7} \times \emptyset_B} \quad \text{(S6)}$$

By combing equation (S3) and (S6), $m_{wet\ cake}$ and $m_{asp,D}$ can be derived to an equation for $m_{asp,D}$;

$$m_{wet\ cake} = \frac{m_{asp,C7} \times \rho_{D/B}}{f_{asp,C7} \times \emptyset_B} + m_{solid} + m_{asp,D} \quad \text{(S7)}$$

$$m_{asp,D} = m_{wet\ cake} - \frac{m_{asp,C7} \times \rho_{D/B}}{f_{asp,C7} \times \emptyset_B} - m_{solid} \quad \text{(S8)}$$

A dry cake sample consists of solids and precipitated asphaltenes due to the diluent and heptane, so the mass of the dry cake, $m_{dry\ cake}$ is

$$m_{dry\ cake} = m_{solid} + m_{asp,D} + m_{asp,C7} \quad \text{(S9)}$$

Thus, from equation (S8) and (S9), $m_{asp,C7}$ can be achieved.

$$m_{dry\ cake} = m_{solid} + m_{wet\ cake} - \frac{m_{asp,C7} \times \rho_{D/B}}{f_{asp,C7} \times \emptyset_B} - m_{solid} + m_{asp,C7} \quad \text{(S10)}$$

$$m_{dry\ cake} = m_{wet\ cake} - \frac{m_{asp,C7} \times \rho_{D/B}}{f_{asp,C7} \times \emptyset_B} + m_{asp,C7} \quad \text{(S11)}$$

$$m_{asp,C7} = \frac{m_{wet\ cake} - m_{dry\ cake}}{\frac{\rho_{D/B}}{f_{asp,C7} \times \emptyset_B} - 1} \quad \text{(S12)}$$

From eq. (S12), in order to estimate the $m_{asp,C7}$ value, the $m_{wet\ cake}$, $m_{dry\ cake}$, $\rho_{D/B}$, $\emptyset_B$, and $f_{asp,C7}$ were needed. The $m_{wet\ cake}$ and $m_{dry\ cake}$ were obtained by weight measurement and both $\rho_{D/B}$ and $\emptyset_B$ were known parameters from the experimental setup. Thus, only $f_{asp,C7}$ was needed to be able estimate the $m_{asp,C7}$. It was assumed that all asphaltenes in the entrapped oil precipitate during washing step. Thus, the $f_{asp,C7}$ was the maximum asphaltenes that can precipitate due to C7, called $f_{asp,C7,max}$, and it was determined by performing additional experiments. The experiments were performed by adding n-heptane into bitumen samples at 40:1 (%wt.), and the solution was used in a similar approach as discussed in Asphaltene Precipitation experiment. It was found that $f_{asp,C7,max}$ of BF1 and BF2 samples were 14.7 ± 0.1%, and BF2 = 14.4 ± 0.1%, respectively. Thus, $m_{asp,C7}$ can be determined and $f_{asp\ and\ solid}$ without entrapped oil effect was estimated. However, in the experiments, some of the asphaltenes precipitated due to adding diluent so $f_{asp,C7}$ should not be the same as the $f_{asp,C7,max}$. Thus, the new $f_{asp,C7}$ was needed using an iterative method. After using $f_{asp,C7,max}$ value in eq. (S12), the $f_{asp\ and\ solid}$ was obtained. This $f_{asp\ and\ solid}$ was corrected with f_{solid} so that $f_{asp,D}$ (mass percentage of precipitated asphaltenes due to diluent) was obtained. This $f_{asp,D}$ represents how much asphaltene precipitated due to the diluent and because $f_{asp,C7,max}$

was known, the new $f_{asp,c7}$ can be estimated using $f_{asp,c7} = f_{asp,C7,max} - f_{asp,\,D}$. The new $f_{asp,c7}$ was used and $f_{asp\ and\ solid}$ was obtained. The process was repeated until the new $f_{asp,c7}$ had the same value as the previous $f_{asp,c7}$. By using this method, $f_{asp\ and\ solid}$ without entrapped oil issue was obtained.

A.2 The First-Order Reaction of the Heterogeneous Nucleation

Following the work by Fávero et al.,[92] heterogeneous nucleation was modeled using a reaction of A→D where A is unstable asphaltenes that can destabilize from the solution and D is deposited asphaltenes on the surface. Fick's first law was used to investigate the heterogeneous nucleation based on the diffusion-limited conclusion from previous work.[20,63,89,92]

First, it is assumed that the mass transport process is at steady state and the one-dimensional Fick's first law is used:

$$J = -D\frac{dC_A}{dx} \tag{S13}$$

Where J [mol/m^2 s] is the molar flux, D [m^2/s] is the diffusivity coefficient, and C_A [mol/m^3] represents the bulk concentration of unstable asphaltenes that have destabilized from the solution, and x [m] is the position in length. Using the thin film approximation to evaluate the concentration derivative above where there is a stagnant thin film surrounding the solid surfaces with a thickness, δ [m], and the concentration at the bulk and surface is C_A and zero, respectively, the flux of asphaltene, J, depositing can be estimated:

$$J = -D\frac{(0 - C_A)}{(\delta - 0)} = \frac{D}{\delta}C_A \tag{S14}$$

To estimate the rate of heterogeneous nucleation, the solid surface area, A [m^2] and total solution volume, V [m^3], were used;

$$-r_{he} = \frac{dC_A}{dt} = \frac{JA}{V} = \frac{D}{\delta}\frac{A}{V}C_A = k_{he}C_A \tag{S15}$$

From eq. (S15), it can be seen that r_{he} can be represented as a first order reaction bulk phase reaction to model the surface deposition processes. The value for A can be determined from $A = S(f_{solid})(g_b)$, where S (m^2/g) is the specific surface area and g_b (g) is the mass of bitumen in the sample. Thus,

$$k_{he} = \frac{D}{\delta}\frac{A}{V} = \frac{D}{\delta}\frac{g_b}{V}S\,(f_{solid}) = \frac{D}{\delta}\emptyset_b\rho_b S\,(f_{solid}) = k_m\emptyset_b\rho_b S\,(f_{solid}) \tag{S16}$$

Where $\emptyset_b$ is the volume fraction of bitumen, ρ_b [g/m^3] is the density of bitumen, and k_m [m/s] is the mass transfer coefficient. Values of k_{he} at different conditions can be estimated assuming that k_m is a constant value.

A.3 Derivation of the Rate of Asphaltene Precipitation

As discussed that the rate of asphaltene precipitation is

$$\frac{dC_A}{dt} = (-k_{ho}C_A^2) + (-k_{he}C_A) \tag{S17}$$

$$-\int_{C_{A_0}}^{C_A}\frac{dC_A}{(k_{ho}C_A + k_{he})C_A} = \int_0^t t \tag{S18}$$

From $\int \frac{1}{x(ax+b)}\,dx = \frac{\ln(\left|\frac{b}{ax+b}-1\right|)}{b} + c$, so

$$-\frac{\ln\left(\left|\frac{k_{he}}{(k_{ho}C_A+k_{he})}-1\right|\right)}{k_{he}}\Bigg|_{C_{A_0}}^{C_A}=t|_0^t \tag{S19}$$

$$\frac{\ln\left(\left|\frac{k_{he}}{(k_{ho}C_{A_0}+k_{he})}-1\right|\right)}{k_{he}}-\frac{\ln\left(\left|\frac{k_{he}}{(k_{ho}C_A+k_{he})}-1\right|\right)}{k_{he}}=t \tag{S20}$$

$$\ln\left(\left|\frac{k_{he}}{(k_{ho}C_{A_0}+k_{he})}-1\right|\right)-\ln\left(\left|\frac{k_{he}}{(k_{ho}C_A+k_{he})}-1\right|\right)=k_{he}t \tag{S21}$$

$$\ln\left(\left|\frac{k_{he}}{(k_{ho}C_A+k_{he})}-1\right|\right)=\ln\left(\left|\frac{k_{he}}{(k_{ho}C_{A_0}+k_{he})}-1\right|\right)-k_{he}t \tag{S22}$$

$$\frac{k_{he}}{(k_{ho}C_A+k_{he})}=\pm e^{\left(\ln\left(\left|\frac{k_{he}}{(k_{ho}C_{A_0}+k_{he})}-1\right|\right)-k_{he}t\right)}+1 \tag{S23}$$

$$C_A=\frac{\frac{k_{he}}{-e^{[(\ln\left|\frac{k_{he}}{k_{ho}C_{A_0}+k_{he}}-1\right|)-k_{he}t]}}-k_{he}}{k_{ho}} \tag{S24}$$

$$C_A=\frac{k_{he}}{k_{ho}}\left\{\frac{1}{-e^{[-k_{he}t+(\ln\left|\frac{k_{he}}{k_{ho}C_{A_0}+k_{he}}-1\right|)]}}-1\right\} \tag{S25}$$

The negative sign of exponential term is used to satisfy the equation.

A.4 Specific Surface Area Estimation

From the SEM images, solid particles were assumed to have a disk shape with radius, r (μm), and height, h (μm). The ImageJ software was used to measure r and h for approximately 10 particles in SEM images. Specific surface area, S (μm^2/g) can be estimated from surface area divided by mass of particle. The surface area, A (μm^2), can be calculated using $A = 2\pi r^2 + 2\pi rh$. The particle mass, m (g), can be obtained from $m = \rho V$ where V (μm^3) is particle volume ($V = \pi r^2 h$) and ρ (g/μm^3) is the particle density.